

**AIRBORNE METEOROLOGICAL MEASUREMENTS COLLECTED
DURING THE MODEL VALIDATION PROGRAM (MVP) FIELD
EXPERIMENTS AT CAPE CANAVERAL, FLORIDA**

Richard M. Eckman
Timothy L. Crawford
Edward J. Dumas
Kevin R. Birdwell

Air Resources Laboratory
Silver Spring, Maryland
August 1999

**AIRBORNE METEOROLOGICAL MEASUREMENTS COLLECTED
DURING THE MODEL VALIDATION PROGRAM (MVP) FIELD
EXPERIMENTS AT CAPE CANAVERAL, FLORIDA**

Richard M. Eckman
Timothy L. Crawford
Edward J. Dumas
Kevin R. Birdwell
Atmospheric Turbulence and Diffusion Division
Oak Ridge, Tennessee

Air Resources Laboratory
Silver Spring, Maryland
August 1999

NOTICE

Mention of a commercial company or product does not constitute an endorsement by NOAA/ERL. Use for publicity or advertising purposes, of information from this publication concerning proprietary products or the tests of such products, is not authorized.

Contents

Executive Summary	v
1. Introduction	1
2. Study Area	3
3. Instrumentation	3
3.1. Aircraft	3
3.2. Sensors	5
3.3. Data Acquisition System	9
3.4. Calibration	13
4. Experiment Design	13
4.1. Session 1	15
4.2. Session 2	17
4.3. Session 3	19
5. Data Processing	20
5.1. Relation Between Probe and Earth Coordinates	22
5.2. Computation of \mathbf{v}_p	25
5.3. Computation of \mathbf{v}_a	26
5.4. Processing of Scalar Quantities	29
5.5. Quality Control	30
5.6. Computer Programs	33
5.7. POD Files	35
5.8. Utility Programs	39
6. Data Collected in Sessions 1–3	40
6.1. Session 1	40
6.2. Session 2	41
6.3. Session 3	45
7. Selected Results	47

8. Summary	51
9. Acknowledgements	52
References	53

Executive Summary

Between July 1995 and May 1996, the U. S. Air Force Model Validation Program (MVP) conducted three field experiments at the Cape Canaveral Air Station, Florida. These experiments were intended to evaluate the dispersion models currently used to support rocket launches at Cape Canaveral. In all three MVP experiment sessions, the Atmospheric Turbulence and Diffusion Division of the NOAA Air Resources Laboratory (NOAA/ARL) deployed an instrumented light aircraft to measure atmospheric variables within and just above the planetary boundary layer. The aircraft is a homebuilt design called a Long-EZ. The sensor array installed on this aircraft is capable of measuring a variety of atmospheric variables, including the mean wind vector, turbulence quantities, vertical fluxes, temperature, humidity, and net radiation. About 165 hours of Long-EZ data were collected during the three MVP sessions.

Hardware problems and weather cancellations limited the amount of aircraft data collected during MVP Session 1 in July 1995. However, the Long-EZ deployments during Sessions 2 (October 1995) and 3 (April–May 1996) were highly successful. The total flight hours for these two sessions met or exceeded expectations, and the data are of high quality.

During MVP, many improvements were made to the software used in processing the raw aircraft data. These improvements were necessary partly because the use of the Long-EZ during MVP was somewhat different than during previous deployments of the aircraft. Many other improvements were made that will benefit future processing of Long-EZ data, including the data from the May 1997 MVP experiment at Vandenberg Air Force Base, California. These improvements include the use of the NetCDF library for machine-independent data storage, the use of enhanced filtering techniques based on Fast Fourier Transforms, and the inclusion of a data quality flag in the processed data. Many of the software improvements developed during MVP have now been generally adopted within the NOAA/ARL aircraft program.

The Long-EZ was an important component of the overall MVP field effort. It was one of the few measurement platforms that could provide turbulence measurements aloft at altitudes where the rocket exhaust clouds typically stabilize after their buoyant rise. Its mobility allowed it to collect measurements over a variety of surface types (land, sea, rivers) within a short period of time. The aircraft measurements will be highly useful for evaluating both the current operational dispersion models and any future models that are developed.

(blank page)

AIRBORNE METEOROLOGICAL MEASUREMENTS COLLECTED DURING THE MODEL VALIDATION PROGRAM (MVP) FIELD EXPERIMENTS AT CAPE CANAVERAL, FLORIDA

Richard M. Eckman
Timothy L. Crawford
Edward J. Dumas
Kevin R. Birdwell

ABSTRACT. Between July 1995 and May 1996, the Model Validation Program (MVP) conducted three field experiments at the Cape Canaveral Air Station, Florida. In all three experiment sessions, the Atmospheric Turbulence and Diffusion Division of the NOAA Air Resources Laboratory deployed an instrumented light aircraft capable of measuring a variety of atmospheric variables, including the mean wind vector, turbulence quantities, vertical fluxes, temperature, humidity, and net radiation. Over the three sessions, approximately 165 hours of aircraft data were collected. These data were obtained over both land and sea, extended throughout the depth of the boundary layer, and covered the time period between early morning and middle evening. The data set will be useful for understanding the atmospheric structure near the Cape, and for evaluating and improving the operational dispersion models used to support rocket launches at the Cape.

1. Introduction

The U. S. Air Force has for many years used a model called REEDM (Rocket Exhaust Effluent Diffusion Model, see Bjorklund 1990) to simulate the dispersion of exhaust clouds produced during rocket launches. These launches take place at the Cape Canaveral Air Station in Florida and Vandenberg Air Force Base in California. Although REEDM has seen extensive operational use, there was concern within the Air Force that it had never been properly peer reviewed and had not been validated using field measurements. As a result, the Model Validation Program (MVP) was formed, its primary goals being to have REEDM reviewed by an external organization and to verify its dispersion estimates using field data (Start and Hoover 1995; Kamada et al. 1997).

Early in the MVP, an external scientific verification and sensitivity study of REEDM was performed (Eckman et al. 1996). Much of the effort in MVP, however, has gone into designing and carrying out a series of field experiments at Cape Canaveral and Vandenberg. It was decided that field experiments were necessary (as opposed to using existing data from other sites) because of the complex environments at the two launch

ranges and the rather unusual nature of the exhaust clouds produced by rocket launches. Both Cape Canaveral and Vandenberg are located in complex coastal environments, so it is difficult to extrapolate the results of idealized experiments over flat, homogeneous terrain to these locations. The exhaust clouds are unusual because of their large initial size and strong buoyancy compared to typical pollutant sources. For Titan IV rockets, currently the largest in the Air Force inventory, the exhaust cloud routinely ascends to 500–1000 m AGL (*e.g.*, Aerospace Corporation 1997a,b) and its initial radius after reaching a stable altitude can approach 500 m.

Three separate MVP experiment sessions have taken place at Cape Canaveral. They were in July 1995 (Session 1), October 1995 (Session 2), and April–May 1996 (Session 3). Each session lasted two to three weeks. Sulfur hexafluoride (SF₆) gas was used as a tracer in all the sessions, and it was released either at the surface near the rocket launch pads or from a blimp circling at a fixed altitude. The elevated releases from the blimp were intended to provide dispersion information at altitudes where the rocket launch clouds typically stabilize. Both puffs and continuous plumes (1–3 hours duration) were released. An attempt was made to conduct releases at various times of the day and night, although for various reasons most of the releases took place during the day. The tracer was sampled aloft with one or two aircraft flying perpendicular to the transport wind direction and at ground level with several vans moving along roads downwind of the release point.

Various other instrument systems were used during the MVP sessions to characterize the meteorology at the time of the tracer releases. Some, such as the Cape tower network and rawinsondes, already existed at the Cape as part of the operational activities. Others were brought in specifically for the MVP sessions, including an instrumented aircraft (distinct from the tracer sampling aircraft), sodars, profilers, and semiportable micrometeorological towers.

Although the main focus of the MVP field studies was to provide validation data for REEDM, there was also an attempt to collect additional data that would be useful in validating more complex models that may replace REEDM in the future. For example, two dispersion modeling systems based on mesoscale flow models are being evaluated at the Cape for possible operational use. The model physics and initialization requirements of these systems are quite different from those of REEDM, so additional field measurements may be useful for validating these models. Some of the field measurements collected during the MVP sessions (*e.g.*, surface fluxes) are not directly applicable for validating REEDM, but would be useful in validating the more complex models.

This report describes the Cape MVP data collected by an instrumented light aircraft operated by the Atmospheric Turbulence and Diffusion Division of NOAA's Air Resources Laboratory. The aircraft is a homebuilt design called a Long-EZ. This aircraft, which was not involved in sampling the SF₆ tracer, is fitted with a large number of instruments that allow it to measure many micrometeorological quantities, including the mean wind vector, turbulence quantities, vertical fluxes, temperature, humidity, and net radiation. The Long-EZ was an important component of the MVP studies because it was the only

platform, other than the Doppler sodars, capable of measuring the turbulence at higher altitudes where the blimp elevated tracer releases took place. Moreover, the aircraft's mobility allowed it to collect micrometeorological measurements in poorly sampled regions such as over the ocean.

This report first describes both the capabilities of the Long-EZ aircraft and the experiment design that was used in operating the aircraft during the three MVP sessions at Cape Canaveral. The postprocessing that is required with the aircraft data is then discussed. Last, an overview of the measurement flights that took place during Sessions 1–3 is provided, including a discussion of overall data quality.

2. Study Area

The study area for MVP Sessions 1–3 was the east coast of Florida near Cape Canaveral. This area is meteorologically quite complex because of the arrangement of land, water and wetlands (Fig. 1). Sea breezes are a common daytime occurrence in the area. Weaker river breezes have also been observed near the banks of the Indian River (Taylor et al. 1989; Zhong et al. 1991; Zhong and Takle 1992). These river breezes may persist for several hours before merging with the general sea-breeze circulation.

Further inland, the surface is a complex mosaic of dry land, lakes, and wetlands. The St. Johns River is a major wetland area running just inland from the coast. The overall surface heterogeneity has a significant effect on surface heat fluxes.

The rocket launch pads are located along the coast near the Cape itself. Major populated areas are mostly located to the west and southwest of the pads. Orlando is located much further inland from the coast.

3. Instrumentation

3.1. Aircraft

The aircraft used to collect micrometeorological measurements during the MVP Cape sessions is a variant of the Rutan Long-EZ (Fig. 2). This is a homebuilt aircraft that flies under an “Experimental” certificate issued by the Federal Aviation Administration. It is a two-passenger aircraft that is built from fiber composites and uses a forward-mounted canard to control pitch rather than the more conventional horizontal stabilizer and elevator combination. The pusher engine configuration is ideal for turbulence measurements, because it allows instruments to be mounted on the nose of the fuselage where they can project into the relatively undisturbed air ahead of the aircraft.

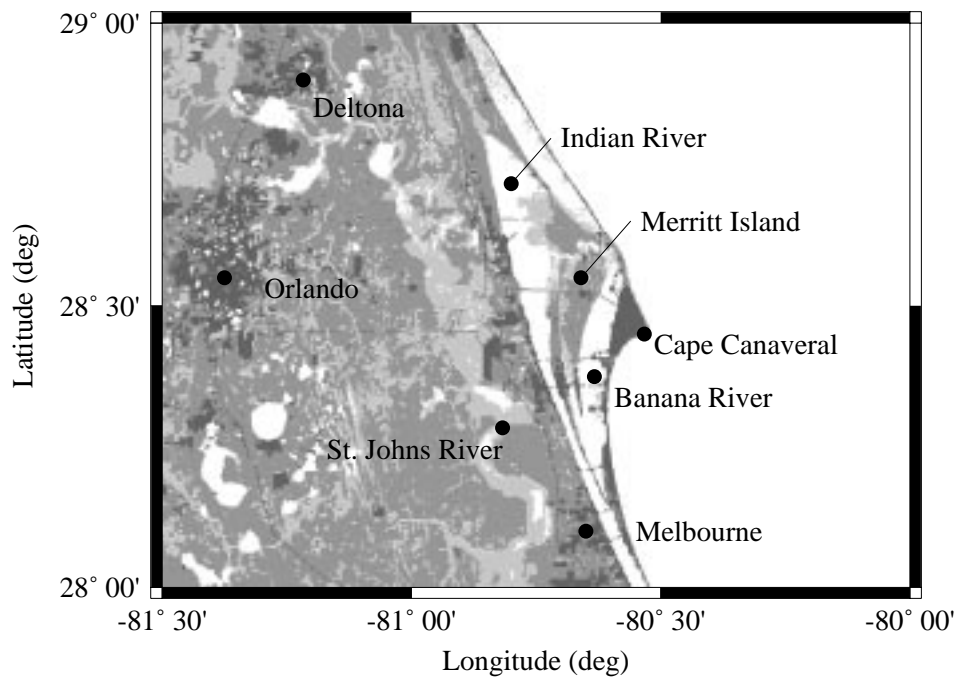


Figure 1: Land-use map of eastern central Florida. The various shades represent water (white), wetlands (lightest grey), forest and fields (intermediate grey), and urban/industrial areas (darkest grey).



Figure 2: The Long-EZ aircraft used during the MVP experiments.

Table 1: Specifications for the Long-EZ aircraft used during the MVP experiments. [Taken from Crawford et al. (1990).]

Empty Weight	430 kg
Gross Weight	725 kg
Powerplant	160 HP Lycoming
Maximum speed	93 m s ⁻¹
Stall speed	27 m s ⁻¹
Ceiling	8000 m
Range	3300 km
Endurance	10–18 hr

Table 1 provides a summary of the Long-EZ’s specifications. Although the top speed is about 93 m s⁻¹, the aircraft was typically flown at speeds of 50–60 m s⁻¹ during data collection.

3.2. Sensors

The Long-EZ carries sensors for measuring a wide variety of atmospheric variables. Some of the sensors are located in a probe extending from the aircraft’s nose. Others are located in a box positioned where the aircraft’s back seat is normally located; this puts the box at the aircraft’s center of gravity. Yet other sensors are scattered at various other locations on the aircraft. The mix of sensors varied somewhat from one MVP session to another, because the system underwent upgrades as new and better hardware became available. A general description of the sensors is given in Crawford et al. (1990), and only a brief overview is given here.

3.2.1. Probe Sensors

The probe on the Long-EZ (Crawford and Dobosy 1992) is mounted on a boom near the aircraft’s nose (Fig. 2) and is designed to extend far enough ahead to sample air that has not been severely disturbed by the aircraft’s presence. It has a hemispherical shape and contains a series of ports (holes) facing forward (Fig. 3). These ports are positioned to measure the pressure distribution over the face of the sphere. When the aircraft is in flight, the total pressure at the ports will vary in a known manner (*e.g.*, Brown et al. 1983; Crawford and Dobosy 1992) related to the relative velocity vector $\hat{\mathbf{v}}_{\mathbf{a}}$, which represents the motion of the air relative to the probe. $\hat{\mathbf{v}}_{\mathbf{a}}$ has three components ($\hat{u}_a, \hat{v}_a, \hat{w}_a$) representing motion along the \hat{x} , \hat{y} , and \hat{z} probe axes as indicated in Fig. 3. A caret is used with these variables to indicate that they are defined in a coordinate system fixed to the probe, rather than one fixed to the earth’s surface.

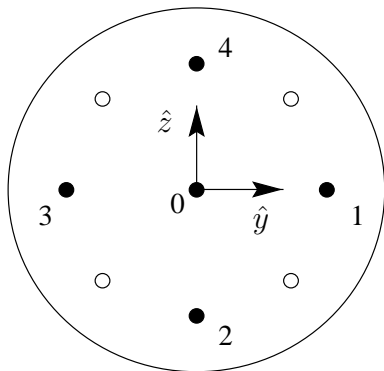


Figure 3: Schematic diagram of the Long-EZ probe as viewed head-on. The ports for both total pressure (filled circles) and static pressure (open circles) are shown. The \hat{x} axis extends out from the page.

Table 2: Specifications for the probe sensors. The data storage rate indicates the frequency at which the data were archived.

Variable	Range	Resolution	Sensor Type or Model	Data Storage Rate (Hz)
P_s	700–1200 mb	0.01%	Setra Systems Model 270	1
δp_s	± 12 mb	0.005 mb	MS-160PC01D36	40
$\delta \hat{p}_x$	0–24 mb	0.005 mb	MS-160PC01D37	40
$\delta \hat{p}_y, \delta \hat{p}_z$	± 12 mb	0.005 mb	MS-160PC01D36	40
T_p	$\pm 15^\circ$ C	0.005 $^\circ$ C	Micro-bead Thermistor	40
\hat{a}_x, \hat{a}_y	$\pm 1 g$	0.0005 g	SenSym-SXL02G	40
\hat{a}_z	+2/ – 1 g	0.007 g	SenSym-SXL02G	40

The four static pressure ports indicated in Fig. 3 are used to measure the static pressure p_s . This pressure is actually measured with a combination of two sensors: one provides a low-frequency reference pressure P_s , and the other is a differential sensor that provides high-frequency fluctuations δp_s . The total static pressure is $p_s = P_s + \delta p_s$. A fast-response differential pressure sensor is used to measure the difference $\delta \hat{p}_x = p_0 - p_s$ between the total pressure p_0 at Port 0 and the static pressure. Two other differential sensors are used to measure the pressure differences $\delta \hat{p}_y = p_3 - p_1$ and $\delta \hat{p}_z = p_2 - p_4$, where p_i is the total pressure at port i . Specifications for the five probe pressure sensors are given in Table 2.

The five probe pressure measurements provide most of the information necessary to estimate the relative wind $\hat{\mathbf{v}}_a$. However, the probe houses other sensors required both for $\hat{\mathbf{v}}_a$ and for estimating the velocity \mathbf{v}_p of the probe relative to the earth’s surface. Probe temperature T_p is measured with a fast-response sensor at Port 0. Three accelerometers are also located within the probe housing. These provide fast-response measurements of the probe’s acceleration vector $(\hat{a}_x, \hat{a}_y, \hat{a}_z)$. The temperature-sensor and accelerometer specifications are listed in Table 2.

Table 3: Specifications for the back-seat sensors. The data storage rate indicates the frequency at which the data were archived.

Variable	Range	Resolution	Model	Data Storage Rate (Hz)
$\hat{a}_{bx}, \hat{a}_{by}$	$\pm 1 g$	$0.0005 g$	Q-Flex	40
\hat{a}_{bz}	$+2/ - 1 g$	$0.007 g$	Systron Donner	40
Pitch†	$\pm 83^\circ$	0.15°	Honeywell JG7044A-35	40
Roll†	$\pm 175^\circ$	0.15°	Honeywell JG7044A-35	40
Yaw rate†	$\pm 6^\circ s^{-1}$	$0.05^\circ s^{-1}$	Honeywell GG13A	40

†: Available only for MVP Sessions 1 and 2

Table 4: Specifications for the GPS systems. No range is given, since the measurements are digital rather than analog.

Variables	Maximum Resolution	Model	Data Storage Rate (Hz)
Velocity	$2 \text{ cm s}^{-1}\dagger$ $20 \text{ cm s}^{-1}\ddagger$	Novatel	1 Sess. 1, 2 10 Sess. 3
Position	$3 \text{ m}\dagger$ $30 \text{ m}\ddagger$	Novatel	1 Sess. 1,2 10 Sess. 3
Attitude Angles	0.05°	Trimble TANS	2 Sess. 1 10 Sess. 2,3

†: Differentially corrected

‡: Not differentially corrected

3.2.2. Back-seat Sensors

A second group of sensors is housed in a box at the aircraft’s center of gravity (CG), a location normally occupied by the aircraft’s back seat. Three accelerometers are used to measure the acceleration vector ($\hat{a}_{bx}, \hat{a}_{by}, \hat{a}_{bz}$) at the CG. During MVP Sessions 1 and 2, gyroscopes were also located at the CG. These provided measurements of the aircraft’s pitch, roll, and yaw rate. The CG sensor specifications are given in Table 3.

3.2.3. GPS system

The Global Positioning System (GPS) was used to provide accurate low-frequency information on the aircraft’s velocity, position, and attitude. Four GPS antennas are located on the aircraft (two along the fuselage centerline and two on the wings). The main GPS hardware is located in the back seat. Two different systems were used: one for positions and velocities and another for attitude angles. Table 4 shows the GPS hardware specifications.

The accuracy of the GPS measurements is greatly enhanced when differential corrections are available (Kruczynski et al. 1985; Leick 1990). To obtain the differential corrections, GPS measurements at a fixed location are required. During MVP, these were collected by a ground station located in a nearby motel room. After a flight was completed, the uncorrected aircraft data were combined with the ground-station data to produce the differentially corrected data. As can be seen from Table 4, the differential corrections increase the accuracy and precision of the velocity and position measurements by roughly an order of magnitude.

3.2.4. Other Sensors

Many additional sensors are mounted on the Long-EZ to provide measurements that supplement the basic wind and turbulence measurements. An Infrared Gas Analyzer (IRGA, Auble and Meyers 1992) is mounted in a housing near the aircraft's nose. This instrument provides fast-response measurements of water-vapor and CO₂ density. A LICOR 6262 gas analyzer was also used on the aircraft to provide slower response measurements of water-vapor and CO₂ concentration. In addition, a chilled mirror was located in a recess on the underside of the fuselage. This instrument provided accurate, slow-response measurements of the dew point temperature T_d . Generally, the IRGA was used for high-frequency water-vapor and CO₂ fluctuations, the chilled mirror was used for baseline humidity measurements, and the LICOR was used for baseline CO₂ concentrations and as a backup humidity sensor to the chilled mirror.

Two temperature sensors are located in a hatch in the aircraft's nose. One provides a fast-response temperature T_h mainly designed to be a backup to the probe temperature T_p . The other is a slow-response sensor that provides an accurate baseline temperature T_b suitable for calibrating the fast-response sensors.

Instruments are also available for measuring radiation-budget variables. A net radiometer is mounted on the aircraft's nose and provides estimates of the net radiation R_n . A pyranometer is mounted on the side of the fuselage to measure upward (PAR_u) and downward (PAR_d) photosynthetically active radiation, which includes radiation having wavelengths between 0.4 and 0.7 μm . Radiative surface temperature T_s is measured with a sensor mounted on the floor of the fuselage.

Supplementary altimeters were also available during some MVP sessions. A slow-response radar altimeter was available during all three sessions, and a laser altimeter was installed during Sessions 2 and 3. These instruments typically only worked properly close to the ground, and were thus not relied upon as the primary source of altitude information. Table 5 provides specifications for the various supplementary sensors.

Table 5: Specifications for the supplementary sensors used on the Long-EZ.

Variables	Range	Resolution	Model	Data Storage Rate (Hz)
Fast H ₂ O & CO ₂	—	10 mg m ⁻³ H ₂ O	IRGA	40
		300 μg m ⁻³ CO ₂		40
Slow H ₂ O & CO ₂	0–12 mmol mol ⁻¹ 300–400 μmol mol ⁻¹	0.02 mmol mol ⁻¹ 0.1 μmol mol ⁻¹	LICOR 6262	1
T_d	±50° C	0.05° C	EG&G	1
T_h	±15° C	0.005° C	Thermistor	40
T_b	-7/+65° C	0.05° C	Platinum sensor	1
R_n	-100/+1200 W m ⁻²	1%	Energy Balance Q*5	1
PAR_u, PAR_d	0–2400 μmol m ⁻² s ⁻¹	1%	LICOR LI-200S	1
T_s	-30/+1200° C	0.1° C	Everest Interscience 4000AH	1
Radar alt.	12–762 m	5%	Terra TRA 3000/TRI30	1
Laser alt.	0–1000 m	10 mm	Riegl LD90-3	40

3.3. Data Acquisition System

Data from the sensors described in Section 3.2. were collected and archived by a computer located at the rear seat of the aircraft. This computer was a personal computer containing a processor from the Intel x86 family and running a version of the DOS operating system. Outputs from the analog sensors (all but the GPS signals) were first passed through a four-pole Butterworth anti-aliasing filter having a cutoff centered at 30 Hz. The signals were then routed to a 12-bit, 32-channel data acquisition board mounted in the computer. The data acquisition board then converted all the analog signals to 200 Hz digital signals.

A computer program called `store`, written in Microsoft QuickBASIC, was used to control the hardware, process the digitized data, and provide visual feedback to the pilot on the status of the system. The treatment given each 200 Hz digital channel depended on whether the channel represented a “fast-response” or “slow-response” sensor. For the fast channels, which are shown with the 40 Hz storage rate in Tables 2–5, the 200 Hz data were block averaged in blocks of five using a triangular filter. The resulting 40 Hz data were then archived. For the slow channels (1 Hz storage in Tables 2–5), the 200 Hz data were first block-averaged to 40 Hz using the same method as the fast channels. These 40 Hz data were then block averaged again to get 1 Hz data. In MVP Sessions 1 and 2, this second level of block averaging was performed using a triangular filter with a span of 2 s; in Session 3, the triangular filter was replaced with a rectangular filter having a span of 1 s.

The GPS data were collected digitally, so they did not go through the data acquisition board. These data come in as individual messages, each having a time tag based on the

Table 6: Raw files generated by the `store` program.

File	Contents
Session 1	
<code>mmddtttt.raw</code>	Fast and slow channels (binary)
<code>mmddtttt.mkr</code>	File marker information (ascii)
<code>mmddtttt.tan</code>	GPS position and velocity (binary)
<code>mmddtttt.tna</code>	GPS angles (binary)
Session 2	
<code>mmddtttt.org</code>	Fast and slow channels (binary)
<code>mmddtttt.mkr</code>	File marker information (ascii)
<code>mmddtttt.tan</code>	GPS position and velocity (binary)
<code>mmddtttt.tna</code>	GPS angles (binary)
Session 3	
<code>mmddtttt.org</code>	Fast and slow channels and some GPS data (binary)
<code>mmddtttt.mkr</code>	File marker information (ascii)
<code>mmddtttt.nov</code>	GPS position and velocity (binary)

highly accurate clocks aboard the GPS satellites. The `store` program decoded these messages and then archived the position, velocity, and attitude-angle data.

The `store` program saved the incoming data on removable disks. In Sessions 1 and 2, these were 230 Mb IOMEGA Corp. Bernoulli cartridges, whereas in Session 3 the system used IOMEGA 100 Mb Zip disks. During a data collection flight, `store` would archive data in several files on the removable disk. The number of files varied from session to session. All the file names followed a `mmddtttt.eee` format, where `mm` is the month, `dd` the day of the month, `tttt` the UTC time, and `eee` is a variable extension. Table 6 lists the raw files created during the three MVP sessions.

The `org` file (`raw` in Session 1) contains all the data from the analog sensors and in Session 3 also contained GPS data that were not differentially corrected. This file is in a binary format specific to the `store` program. The first part of the file is a header that contains basic information about the data, such as the start and end times, number of data records, and record size. After the header, the data are stored in individual records called scans. Each scan contains one second of data. The `store` program used a data structure called `StoreType` to hold each scan's data in memory, and the data in the `org` file are images of this structure. The `StoreType` structure differed for each session. The structure for Session 3, presented as a C-language structure, is given below as an example:

```
struct StoreType
{
    short F[40][nfast];
```

```

    short S[nslow];
    short GPS[10][ngps];
    int time;
};

```

All the data but `time` are 2-byte short integers. This reduces the storage space required for the data. Scales and offsets obtained from the file header are used to convert these integers to floating-point values with the correct units. Array `F` contains the 40 Hz data. The first array index `nfast` denotes the data channel, and the second index spans the 40 values available each second. Array `S` holds the slow channels (only one value per scan). Array `GPS` holds GPS data for the scan, in this case 10 values per scan. The `ngps` index denotes the GPS data channel.

The `tan` and `tna` files in Sessions 1 and 2 contained the GPS position, velocity, and angle data together with the information required to differentially correct the positions and velocities. One limitation of the `store` program during these sessions was that no attempt was made to synchronize the GPS and analog data streams in time. Instead, the data streams were diverted to separate files (`raw/org` vs. `tan` and `tna`), and time synchronization was left as a postprocessing step. For Session 3, a newer version of `store` was used that did attempt to synchronize the GPS and analog streams. This was done using the time tags present in each message coming from the GPS subsystems. Because of this synchronization, it was possible to directly place the GPS data into the `org` file in Session 3, the one limitation being that the positions and velocities were not differentially corrected. The `nov` file contained the data necessary for performing the differential corrections in postprocessing.

The marker `mkr` file is an ascii file that helps to describe what the aircraft was doing during specific parts of a flight. Prior to a flight, the pilot was given a flight plan describing the locations and altitudes where data should be collected. The flight plan described a sequence of actions, such as “fly from point *A* to point *B* at 100 ft, reverse course and fly *B*–*A* at 300 ft, then fly to point *C* and fly from *C* to point *D* at 100 ft”. In this example, there are three actions (*A*–*B*, *B*–*A*, and *C*–*D*) designed to collect data at locations of specific scientific interest. However, the aircraft must spend part of the time maneuvering between the actions. Data are still being collected during these maneuvering periods, but these data are not the primary focus of the flight. The marker file is used to indicate when the aircraft was performing an action in the flight plan and when the aircraft was maneuvering between actions.

The `mkr` file contains a series of entries that describe when a specific action in the flight plan was started and completed. These entries are created when the pilot toggles a switch in the cockpit. The pilot first toggles the switch at the start of a flight-plan action. This places one marker (*i.e.*, entry) in the `mkr` file. At the completion of the action, the pilot toggles the switch again, creating another marker in the file. The beginning and ending markers together form what is called a marker pair, which delineates one specific action.

An excerpt from a `mkr` file is given below:

```
XXX -1 2247 05031411 15:00:32 28.404 -80.655
      0 2469 05031411 15:04:14 28.503 -80.614
XXX -1 2646 05031411 15:07:11 28.513 -80.615
      0 2872 05031411 15:10:57 28.411 -80.650
XXX -1 3029 05031411 15:13:34 28.400 -80.656
      0 3237 05031411 15:17:02 28.503 -80.613
```

This example has three marker pairs. The beginning marker of each pair has seven fields. Field 1 is a three-character identifier that defaults to “XXX”, but can be replaced by other characters if desired. This identifier is solely for documentation purposes. Field 2 is always “-1” to indicate that this is the first marker of a pair. Field 3 is the scan number where the marker was toggled. This identifies exactly where in the data files the pilot toggled the marker switch. Field 4 is the date and time (UTC) when the data files were opened. The date and time are given in a MMDDTTTT format, where MM is month, DD is day, and TTTT is the time. Field 5 is the time in hours, minutes, and seconds (UTC) when the marker was toggled. The last two fields are the aircraft’s GPS latitude and longitude in decimal degrees at the time the marker was toggled.

The ending marker has one less field than the beginning marker. Field 1 is always “0” to indicate an ending marker. The remaining fields are the same as in the beginning marker. In the example above, there are three marker pairs spanning scans 2247–2469, 2646–2872, and 3029–3237. These could, for example, represent the flight legs $A-B$, $B-A$, and $C-D$ mentioned earlier in this section. Note that a 177 s gap exists between the first and second marker pair, and a 157 s gap is present between the second and third pairs. This represents the time required in maneuvering the aircraft into position for the next action in the flight plan.

The `mkr` file entries are largely based on the flight plan provided to the pilot prior to the flight. The flight plan, in turn, was devised to provide certain scientific measurements useful to MVP. However, an investigator can easily edit or even replace the original `mkr` file if this proves to be useful. (The only real limitation here is that the scan numbers listed in the `mkr` file must not exceed the total number of scans available in the data.) An example might be a researcher who wanted to use MVP data for an unrelated project having different goals than MVP. Parts of the flight that were of limited interest to MVP may be of great interest for this project, so alterations of the original `mkr` file may be warranted. As far as the data postprocessing, the primary function of the `mkr` file is to organize the computation of turbulence statistics (see Section 5.8.).

3.4. Calibration

Most of the sensors used on the Long-EZ have stable calibrations that do not drift over time. These sensors were calibrated in the laboratory prior to deployment in the field. Periodically, these sensors are recalibrated to ensure their accuracy. The pressure, acceleration, and radiation sensors; the chilled mirror; the slow-response temperature; and the gyroscopes fall into this category.

The IRGA is more complex, because its response to water-vapor density is nonlinear (Auble and Meyers 1992). Additionally, this sensor suffers from a base-line drift that makes it suitable for measuring fast-response fluctuations but not for obtaining absolute measurements of water-vapor density. During postprocessing, the IRGA water-vapor calibration was recomputed for each flight using the chilled-mirror T_d measurements as a reference. The procedure is described in more detail in Section 5.4.

The calibrations for the fast-response temperatures T_p and T_h were also recomputed during postprocessing for each flight using T_b as a reference. These sensors actually have stable calibrations, so the recalibrations were mainly used to ensure that exterior factors such as insect strikes had not altered the calibrations. The reason these sensors were singled out for this treatment is that the Long-EZ's primary focus in earlier field experiments (before MVP) was in computing the sensible and latent turbulent heat fluxes. Some additional effort was therefore made to ensure accurate calibrations for the temperature fluctuations. The T_p and T_h calibrations generally varied little during the MVP sessions.

4. Experiment Design

The Long-EZ measurements were just one component of the overall MVP effort (Start and Hoover 1995; Kamada et al. 1997). Their main role was to provide information on the horizontal and vertical variations of the winds and turbulence in the Cape Canaveral area. This included measurements that would be useful in characterizing the effect of sea breezes on the wind and turbulence fields. As a secondary role, the Long-EZ collected measurements of the vertical turbulent fluxes and radiation budget, which would be useful in evaluating mesoscale-model simulations at Cape Canaveral.

The main component of the experiment design for the Long-EZ was the development of a flight plan for each flight. This flight plan was a set of instructions to the pilot describing locations and altitudes at which the Long-EZ should be flown for data collection. Typically, the flight plan listed a series of straight line segments that should be flown sequentially at specified altitudes. Each segment was designed to measure a particular aspect of the flow near the Cape. The development of the flight plans was affected by three considerations: the scientific objectives of the flight, coordination with the other MVP assets, and the safe operation of the aircraft within the Federal Aviation Regulations (FARs).

The scientific objectives of the Long-EZ flights varied somewhat from one MVP session to another. This was mainly due to differences in the prevailing meteorology during the three sessions. The scientific objectives are described more fully later in the individual subsections for each session.

The Long-EZ flights were closely coordinated with the other vehicles and instrumentation operating during MVP. Throughout all the sessions, the primary focus each day was on the SF₆ tracer releases (Kamada et al. 1997). These releases took place either at the surface or from a blimp circling at heights up to 1200 m MSL. Both plume releases of about two hours duration and quasi-instantaneous puffs were released. On many days, an ambitious schedule of two or three continuous releases was attempted, although this was sometimes not obtained in practice. The Long-EZ flight plans were designed to provide data in a time window that encompassed the tracer releases. Usually, the aircraft started collecting data at the start of a tracer release and continued for 3–4 hours thereafter. On a few occasions the Long-EZ collected data when no tracer releases were ongoing. This usually happened when the tracer release was canceled after the Long-EZ was airborne.

Coordination also included avoiding conflicts with other MVP aircraft. The blimp was easy to avoid, because it is big and slow. But MVP also employed one or two other fixed-wing aircraft that were used to sample the SF₆ downwind of the release point. These aircraft usually flew perpendicular to the plume centerline. To avoid conflicts, the Long-EZ normally did not collect data directly downwind from the release point. The one exception was that at the beginning of many tracer releases, the Long-EZ flew a “downwind radial” at the tracer release height. The radial started near the release point and extended 10–15 km in the estimated downwind direction. The intent was to characterize the wind and turbulence along the tracer’s transport route. After completing the downwind radial (it only required a few minutes), the Long-EZ cleared the tracer-release area.

The FARs placed a number of restraints on the Long-EZ’s operation. The airspace around Cape Canaveral is rather congested and contains many regions of controlled airspace. Orlando International Airport, about 90 km west of the Cape, has several layers of controlled airspace extending almost to the East Coast of Florida. This limited how far inland the Long-EZ could fly, and also restricted altitudes to less than 6000 ft (1828 m) MSL over many inland areas. Space Center Executive Airport also has some controlled airspace extending from the surface to 2500 ft (762 m) MSL. To the south, Patrick Air Force Base has its own controlled airspace. Cape Canaveral itself has a number of restricted areas covering the areas affected by rocket launches. Some of these restricted areas are only activated when launches or other government flight activities are taking place, whereas others are active continuously. Usually, the restricted areas over the Cape could be entered after obtaining a clearance from air traffic control.

The FARs also placed a limitation on minimum altitudes. Generally, a minimum altitude of 1000 ft (305 m) AGL is required over densely populated areas, and a 500 ft (152 m) AGL minimum is required over other populated areas. Lower altitudes are allowed under certain circumstances in unpopulated or sparsely populated areas. These altitude limitations

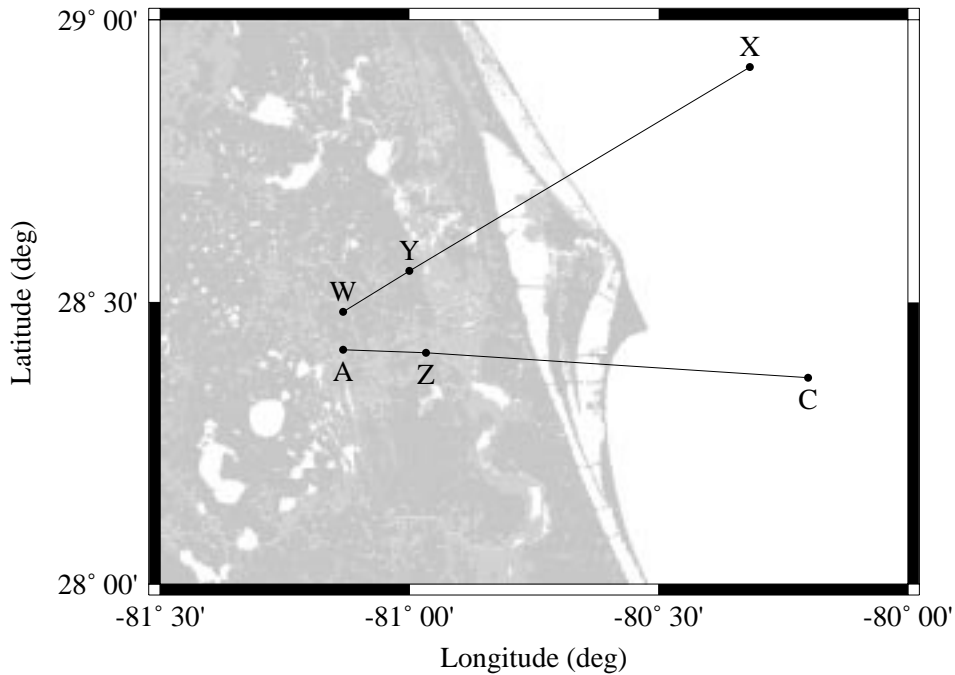


Figure 4: Aircraft transects used during MVP Session 1. Waypoints are denoted by letters.

strongly restricted the areas where low-level measurements of turbulent fluxes could be collected.

Given the operational limitations described above, the Long-EZ flight plans were developed to address specific scientific issues of relevance to MVP. The scientific objectives differed somewhat for each of the three sessions, as discussed in the following subsections.

4.1. Session 1

Session 1 took place during the summer (July 1995), when sea breezes and afternoon thunderstorm development are significant factors over the Florida Peninsula (Byers and Rodebush 1948; Neumann 1971; Reed 1979; Atkins et al. 1995; Atkins and Wakimoto 1997). Since the major horizontal variations in sea-breeze structure occur along an axis perpendicular to the coast, the experiment plan during Session 1 focused on having the aircraft fly transects perpendicular to the coast. The two transects used during the session are shown in Figure 4. They are both approximately 93 km in length. Positions for the waypoints are given in Table 7.

Table 7: Locations of waypoints used in MVP Session 1.

Waypoint	Latitude	Longitude
A	28°25'00"	-81°08'00"
C	28°22'00"	-80°12'00"
H	28°41'00"	-81°03'00"
J	28°33'00"	-80°59'00"
K	28°40'00"	-80°58'00"
L	28°41'00"	-80°51'00"
M	28°47'00"	-80°52'00"
O	28°49'00"	-80°44'00"
P	28°49'00"	-80°35'00"
Q	28°42'00"	-80°29'00"
U	28°36'00"	-80°45'00"
W	28°29'00"	-81°08'00"
X	28°55'00"	-80°19'00"
Y	28°33'20"	-81°00'00"
Z	28°24'40"	-80°58'00"

At the typical airspeeds used by the Long-EZ during data collection, each transect required about 30 minutes to complete. This limited the number of altitudes that could be flown within the time frame of a single SF₆ tracer release. Usually, the transects were flown at only two altitudes. Low-level runs were flown at about 160–200 m MSL to characterize the sea-breeze circulation near the surface. Higher level runs were flown in an attempt to characterize the return flow of the sea breeze. Because of the structure of the controlled airspace around Orlando International Airport, these runs were typically flown at 1500–1600 m MSL along the Z–C and Y–X portions of the transects, and at somewhat lower altitudes of 800–850 m along A–Z and W–Y.

In addition to the sea-breeze transects illustrated in Fig. 4, the Long-EZ on two days also flew a “flux run”. This type of flight was designed to obtain surface-flux measurements over different kinds of surface. Waypoints used during the flux runs are shown in Fig 5. The H–M portion of the run is intended to obtain flux measurements over different land surfaces, whereas the O–Q portion is of course for fluxes over the sea. The M–O portion was intended for determining the fluxes over the inland waterways. A major consideration in developing the flux run was to obtain flux measurements over as many different surfaces as possible while remaining clear of populated areas. This explains the rather convoluted nature of the legs in Fig. 5.

Two other patterns were flown during some flights: box patterns and spiral ascents. These were designed to directly support the tracer releases. In a box pattern, the aircraft flew at a fixed altitude along a more or less rectangular path. Usually, the box was flown close to

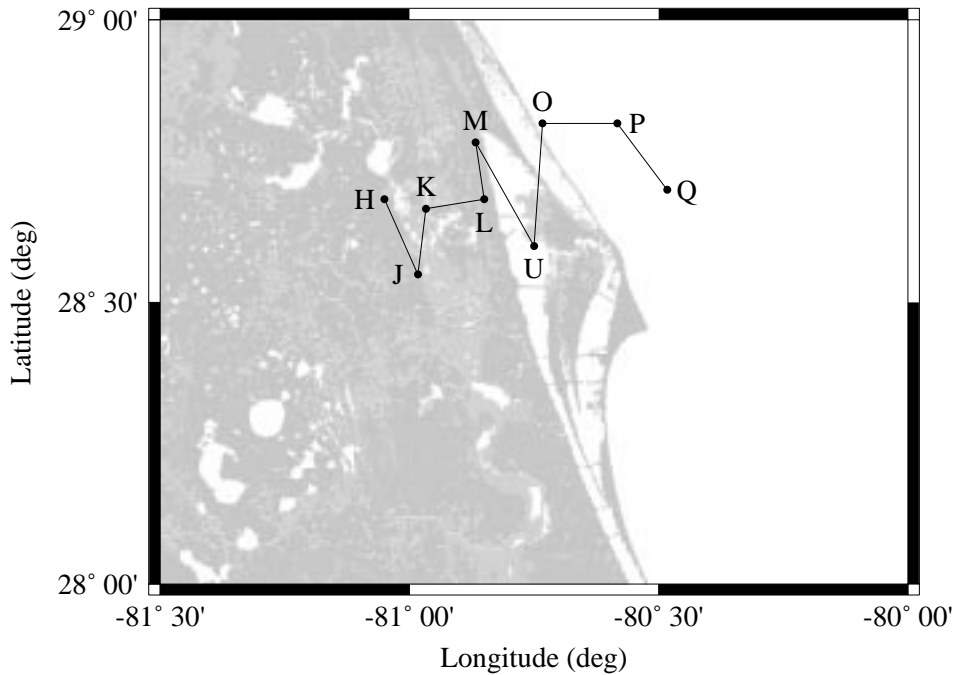


Figure 5: Aircraft waypoints used for flux measurements.

the SF₆ tracer release point, both in horizontal position and in altitude. The intent was to obtain wind and turbulence data near the tracer release point. In a spiral ascent, the pilot flew along a roughly circular path while in a steady climb. This was initiated near the surface and continued up to about 1500 m MSL.

One problem with the box patterns and spiral ascents was that the aircraft spent a considerable fraction of the time turning. With the hardware and software that was used during Session 1, it is unclear whether the system could collect reliable wind data during turns. Data from other experiments indicated that the quality of the wind data tended to deteriorate as the turn steepened. Also, the field of view of the radiation sensors is affected in a turn. The temperature and humidity data were not affected by the turns.

4.2. Session 2

The experience gained during Session 1 led to some changes in the experiment design for Session 2 in November 1995. Having the aircraft fly long transects perpendicular to the coast turned out to be not the best way to employ the aircraft, in part because there was not sufficient time to fly enough different altitudes to provide a reasonable vertical profile of the flow. Other important factors in Session 2 were that sea breezes were less frequent, and the synoptic flow had a stronger influence.

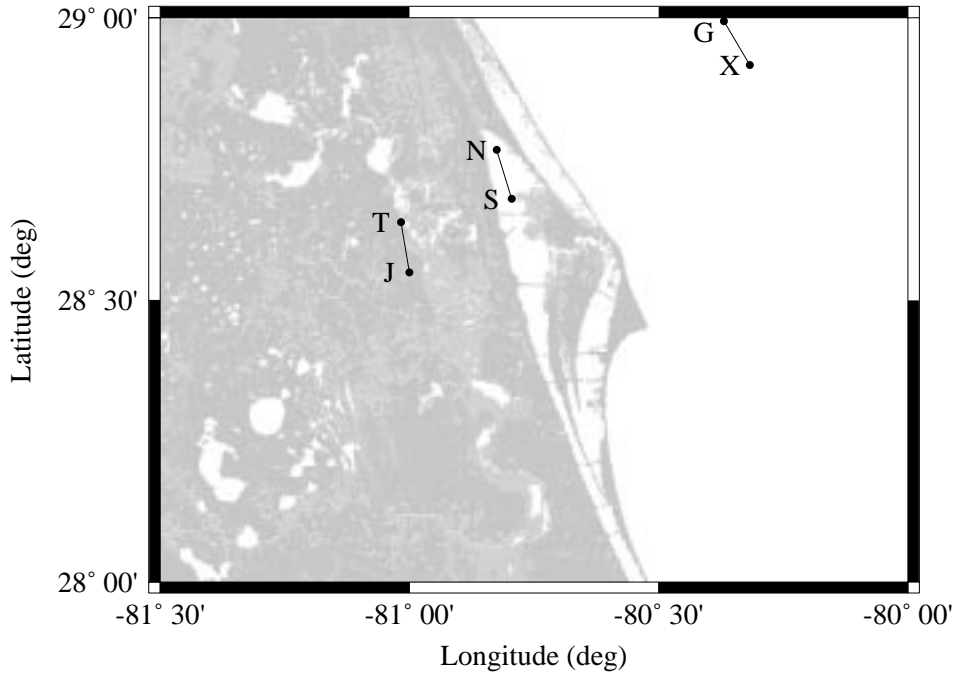


Figure 6: Aircraft waypoints for MVP Session 2.

For Session 2, it was decided to base the flight planning on a series of shorter transects oriented more or less parallel to the coastline. Since each transect is shorter, several different altitudes could be flown in a reasonable amount of time. The reason for aligning the transects parallel to the coast was that the turbulence along the transect should be as homogeneous as possible, which would be useful for computing robust turbulence statistics.

The Long-EZ flights during Session 2 were largely based on the waypoints shown in Fig. 6, with the corresponding latitudes and longitudes of the waypoints given in Table 8. Each of the three legs shown (T–J, N–S, and G–X) is about 10 km in length, which provides a reasonably long sample for computing turbulence measurements while keeping the total time required to fly each leg down to about 3–4 minutes. The T–J leg was intended to characterize the boundary-layer structure over land, N–S was intended to characterize the structure over an inland waterway (Indian River), and G–X was for measurements over the ocean. In flying between these legs, the aircraft followed a course similar to the W–X leg in Fig. 4. Thus, some information similar to what was obtained in Session 1 was still available in the Session 2 data, with the significant advantage that much better vertical information was available at the three legs in Fig. 6.

Each flight leg was usually flown at several different altitudes in succession. The most common altitudes were 30, 150, 275, 520, 915, and 1675 m MSL. Except for the 30 m altitude, these follow a roughly logarithmic progression. These altitudes were commonly

Table 8: Locations of waypoints used in MVP Session 2.

Waypoint	Latitude	Longitude
G	28°59'39"	-80°22'08"
J	28°33'00"	-81°00'00"
N	28°46'00"	-80°49'30"
S	28°40'50"	-80°47'42"
T	28°38'20"	-81°01'00"
X	28°55'00"	-80°19'00"

Table 9: Locations of waypoints used in MVP Session 3.

Waypoint	Latitude	Longitude
D	28°46'00"	-80°31'00"
E	28°51'30"	-80°35'00"
J	28°33'00"	-81°00'00"
N	28°46'00"	-80°49'30"
S	28°40'50"	-80°47'42"
T	28°38'20"	-81°01'00"
U	28°36'00"	-80°45'00"

used during the day under convective conditions. During the few flights under more stable conditions, the aircraft stayed closer to the surface, since the boundary layer was not as deep.

On many flights, the Long-EZ spent some time collecting fluxes over the ocean. This was done when the aircraft was in transit between the base airport and the G–X leg. Instead of simply wasting this transit time, it was decided to have the aircraft fly low to the surface to collect flux measurements over the ocean.

4.3. Session 3

During Session 3 in April and May 1996, sea breezes were again an important consideration for MVP. Because of the success with the basic experiment design in Session 2, many of the Session 3 flights were based on a similar set of waypoints, as shown in Fig. 7 and Table 9. The T–J and N–S legs are the same as in Session 2. The U waypoint was added as an extension to N–S that added some measurements over the western edge of Merritt Island. For this session, the D–E leg was used for collecting measurements over the ocean. A significant advantage of this leg was that the transit time in reaching the leg was considerably reduced compared with the G–X leg from Session 2. Generally, the legs shown in Fig. 7 were flown at the same altitudes used in Session 2.

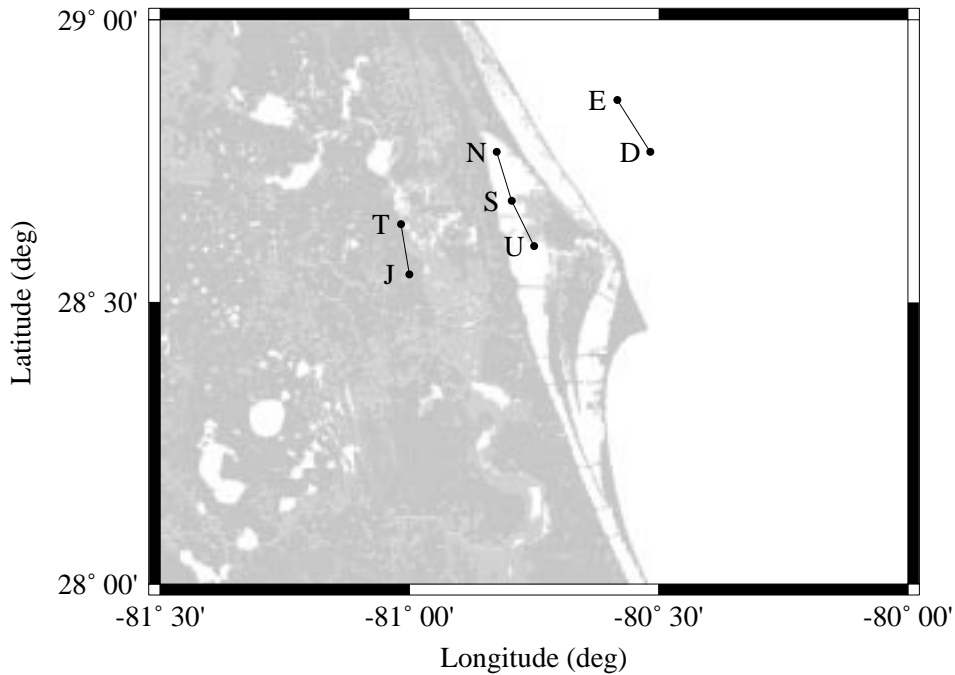


Figure 7: Aircraft waypoints for MVP Session 3.

Another phenomenon that was of considerable interest during MVP Session 3 was the development of convergence zones over Merritt Island during the day. From Fig.1 it is seen that Merritt Island has the ocean to the east, and inland waterways to the south and west. The differential heating of the island relative to the surrounding water can cause the development of a convergence zone over the island (*e.g.*, Zhong et al. 1991; Simpson 1994; Kamada et al. 1997). This convergence zone was sometimes visible as a line of cumulus clouds (Kamada et al. 1997).

A series of flight legs (Fig. 8) were developed to investigate the Merritt Island convergence zone. The positions of the waypoints are given in Table 10. The intent was to have three legs that span the eastern, central, and western portions of the island. For legs CZ3–CZ4 and CZ5–CZ6, the underlying areas were populated, so the aircraft had to remain at least 500 ft (150 m) above the ground. CZ1–CZ2 was over water, so the aircraft could fly lower on this leg.

5. Data Processing

One aspect of the Long-EZ's instrumentation system is that a considerable amount of postprocessing is required to convert the raw data to a form that is directly useful for

Table 10: Waypoints used during investigations of the Merritt Island convergence zone.

Waypoint	Latitude	Longitude
CZ1	28°30'00"	-80°37'00"
CZ2	28°24'45"	-80°39'00"
CZ3	28°30'30"	-80°40'00"
CZ4	28°24'45"	-80°40'45"
CZ5	28°30'30"	-80°42'30"
CZ6	28°24'45"	-80°43'00"

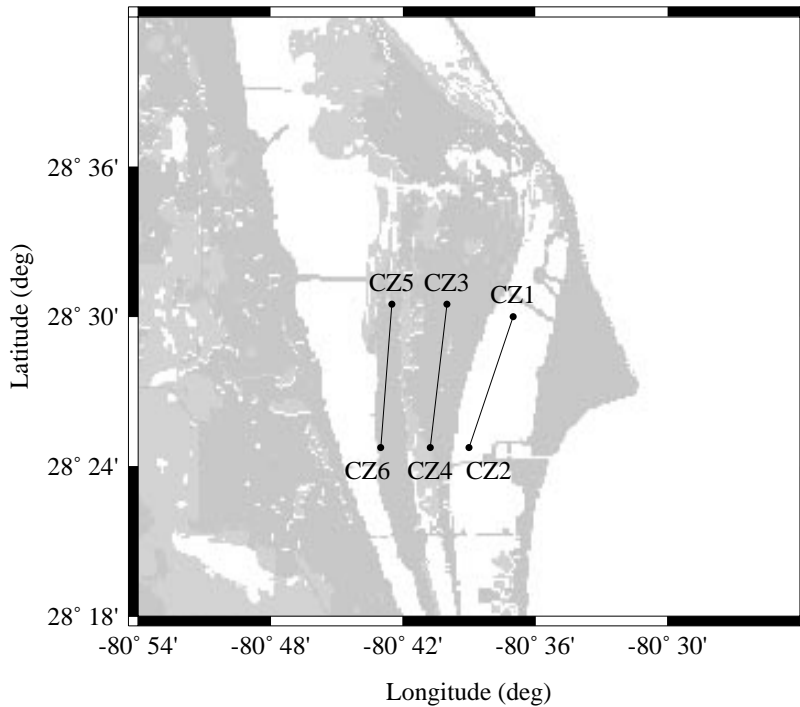


Figure 8: Waypoints used to investigate Merritt Island convergence zone during MVP Session 3.

scientific investigation. The raw data include pressure and temperature fluctuations, accelerations, and aircraft positions and orientation angles from the GPS subsystem. These must be converted to the ambient wind fluctuations that are required for computing the mean wind vector and various turbulence and flux quantities. This section describes the postprocessing applied to the MVP raw data.

As discussed in Section 3.3., the raw data includes fast-response sensors archived at 40 Hz, slow-response sensors archived at 1 Hz, and GPS measurements archived at a variety of rates. In the processed data, all the variables are stored at either 1 or 40 Hz. The 1 Hz “slow” variables are mainly intended to provide mean values, whereas the 40 Hz “fast” variables are intended to provide sufficient spatial resolution for computing turbulence and flux statistics. At the typical air speeds used by the Long-EZ, 40 Hz theoretically allows the system to resolve spatial scales along the flight path down to about 2.5 m.

The most complex aspect of the data processing is the computation of the ambient wind vector \mathbf{v} from the raw pressure, acceleration, gyroscope, and GPS measurements. This vector is defined in a coordinate system with a fixed orientation relative to the earth, rather than in one oriented with the aircraft. \mathbf{v} can be computed by noting that the difference between it and the velocity \mathbf{v}_p of the aircraft probe relative to the earth is equal to the velocity \mathbf{v}_a of the air relative to the probe:

$$\mathbf{v} - \mathbf{v}_p = \mathbf{v}_a \tag{1}$$

For all three vectors, it is assumed for convenience that the positive x axis is east, the positive y axis is north, and the z axis is vertical. [\mathbf{v}_a in Eq. (1) and $\hat{\mathbf{v}}_a$ in Section 3.2.1. are the same quantity in different coordinates: \mathbf{v}_a is oriented with the earth-fixed coordinate system (x, y, z) , whereas $\hat{\mathbf{v}}_a$ is in the probe coordinate system $(\hat{x}, \hat{y}, \hat{z})$.] The basic conceptual design of the Long-EZ’s instrumentation system is to measure \mathbf{v}_p and \mathbf{v}_a separately and then use Eq. (1) to obtain \mathbf{v} . The following subsections describe the computations of \mathbf{v}_p and \mathbf{v}_a in more detail. Later subsections describe the processing of other measured variables and the format used to store the processed data.

5.1. Relation Between Probe and Earth Coordinates

Some of the aircraft sensors, such as the GPS subsystem, provide vector quantities that are oriented in the earth coordinate system (x, y, z) . Others, such as the probe sensors, produce vectors in the probe coordinates $(\hat{x}, \hat{y}, \hat{z})$. The relationship between these coordinate systems varies with time and must be measured so that the proper rotations can be applied to vector quantities. Three angles are used to express the relative orientation of the two systems: the roll ϕ , pitch θ , and yaw ψ . Rotations such as these in three dimensions are not commutative, so the three rotations cannot be applied in arbitrary order. In transforming from probe to earth coordinates, the rotations are applied in the order ϕ , θ , and ψ .

The roll angle ϕ represents a rotation about the probe \hat{x} axis. The convention used here is that ϕ is zero when the probe \hat{y} axis is level with the horizon and the \hat{z} axis is pointing up

(in case the pilot is collecting measurements while flying inverted). A positive change in the roll angle occurs when the \hat{y} axis is rotated clockwise while viewing the probe head-on as in Fig. 3 (*i.e.*, a roll to the left from the pilot's perspective). The pitch angle θ represents a rotation about the probe \hat{y} axis (with the qualification that the ϕ rotation must be applied first). Similar to the roll, $\theta = 0$ when the \hat{x} axis is level with the horizon. A positive pitch angle is present when the positive \hat{x} axis points above the horizon. After the roll and pitch rotations are applied, the yaw angle ψ represents rotation about the \hat{z} axis. The yaw angle is zero with the \hat{x} axis pointing east and is considered to be positive when measured in a clockwise direction from due east.

All three attitude angles are provided directly by the GPS subsystem. However, the GPS data during the MVP sessions did not provide the angles at the 40 Hz rate (see Table 4) required to rotate any of the fast variables. The GPS data were therefore combined with faster response data from the gyroscopes and accelerometers to produce composite 40 Hz time series of the attitude angles. Gyroscopes were only used during Sessions 1 and 2. They provided 40 Hz measurements of ϕ , θ , and the yaw rate $\partial\psi/\partial t$, where t is time.

The accelerometers could also be used to obtain attitude-angle data by looking at differences between the probe and back-seat accelerations. The difference between \hat{a}_z and \hat{a}_{bz} , for example, is related to the pitch through the relation

$$\frac{\partial^2\theta}{\partial t^2} = \frac{\hat{a}_z - \hat{a}_{bz}}{d}, \quad (2)$$

where d is the distance from the probe to the back seat. Likewise, the yaw is related to the \hat{y} accelerations through

$$\frac{\partial^2\psi}{\partial t^2} = -\frac{\hat{a}_y - \hat{a}_{by}}{d}. \quad (3)$$

Because a double integration is required to obtain θ and ψ from these equations, any acceleration errors at low frequencies are greatly magnified in θ and ψ . Hence, only the high-frequency fluctuations from the accelerometers are used.

For all three MVP sessions, Eqs. (2) and (3) were used to provide the high-frequency fluctuations for θ and ψ . In Sessions 1 and 2, the gyroscopes were used as the high-frequency reference for ϕ . No gyroscopes were available in Session 3, so the 10 Hz GPS measurements were the sole source of roll data. It was assumed that there were no significant roll fluctuations between 5 Hz (the GPS Nyquist frequency) and 20 Hz (the Nyquist frequency for 40 Hz data), which is a reasonable assumption for the Long-EZ.

The GPS angles were combined with the gyroscope/accelerometer data to create a 40 Hz blended set of angles ϕ , θ , and ψ . The GPS data were assumed to provide the low-frequency references ϕ_ℓ , θ_ℓ , and ψ_ℓ , whereas the gyroscope/accelerometers provided the high-frequency references ϕ_h , θ_h , and ψ_h . These signals were blended in frequency space by taking the Fourier transform of all the time series. Using the Fourier transform $\Theta(f)$ of the pitch θ at frequency f as an example, the blending took the form

$$\Theta(f) = (1 - \eta) \Theta_\ell(f) + \eta \Theta_h(f), \quad (4)$$

Table 11: Filtering frequencies f_1 and f_2 used for the attitude angles during MVP.

Session	f_1 (Hz)	f_2 (Hz)
1	0.19	0.33
2	0.75	1.33
3	0.75	1.33

where $\eta = \eta(f)$ is a weighting function between 0 and 1. Below a specified frequency f_1 , η was set equal to zero. Above another frequency f_2 ($> f_1$), η was unity. At frequencies f between f_1 and f_2 , the weighting function took the form

$$\eta = \frac{\log(f/f_1)}{\log(f_2/f_1)}. \quad (5)$$

With a logarithmic frequency axis, η has a simple shape in that it is zero below f_1 , ramps up to 1 between f_1 and f_2 , and then remains at 1 thereafter. The filtering is symmetric in that negative frequencies are treated the same as positive frequencies.

The reason the filter is allowed to ramp between f_1 and f_2 is to avoid making the cutoff of the filter too sharp. Usually, these frequencies were defined so that they spanned a quarter decade: $\log(f_2/f_1) = 0.25$. The values used for the three MVP sessions are given in Table 11. These were chosen to ensure f_2 remained below the Nyquist frequency of the GPS data and also to account for data losses resulting from problems with the data acquisition system. The frequencies used for Session 1 fall well short of the 1 Hz Nyquist frequency expected from the GPS system, because data losses pushed the effective Nyquist frequency below 1 Hz. The Session 2 and 3 frequencies are centered at 1 Hz.

The use of Fourier transforms in blending the GPS and gyroscope/accelerometer data had another benefit in dealing with the accelerometer data. As shown in Eqs.(2) and (3), the accelerometers provide the second derivatives of the pitch and yaw angles. The usual approach would be to doubly integrate these equations in time using a numerical approximation. However, these integrations become much simpler to carry out after Fourier transformation, because integration in time becomes simple multiplication in frequency. Thus, the integrations in Eqs.(2) and (3) were performed by first taking the Fourier transform of the right sides, and then multiplying the resulting Fourier coefficients by the filter function

$$I(f) = \frac{1}{(2\pi f)^2}. \quad (6)$$

The filtered coefficients then represent the Fourier transforms of θ and ψ .

After the filtering and blending described above were completed, the resulting Fourier transforms were inverse transformed to their corresponding angles ϕ , θ , and ψ . These 40 Hz blended angles are the ones that are used to rotate vectors from the probe coordinate system to earth coordinates.

5.2. Computation of \mathbf{v}_p

The primary source of the probe velocity \mathbf{v}_p measurements on the Long-EZ was the GPS subsystem. The GPS provides direct measurements of the probe velocity in a digital form. Using these data is straightforward except for two problems. First, the raw GPS velocity measurements do not have adequate accuracy (Table 4) for measuring turbulent velocity fluctuations. Second, the GPS velocities have the same problem as the attitude angles described in the foregoing section, namely that they did not have a fast enough sampling rate to provide \mathbf{v}_p measurements up to the desired 40 Hz.

The first problem was addressed by using differential corrections (Kruczynski et al. 1985; Leick 1990) to improve the accuracy of the GPS velocity (and position) data. In this approach, a second GPS receiver—the ground station—is operated concurrently with the receiver on the aircraft. This second receiver remains at a fixed location. As long as the aircraft does not fly too far from the ground station, many GPS errors will equally affect both receivers and can therefore be subtracted out, providing significant improvements in accuracy. With the system used on the Long-EZ, the differential corrections increase the GPS accuracy by roughly a factor of 10, providing up to 2 cm s^{-1} accuracy in the velocity.

During MVP, the ground station was located at a motel in Cocoa Beach, just to the south of the Cape. A desktop computer collected data from a GPS antenna on the roof of the motel and archived the data at 2 Hz. The system was started just before the Long-EZ took off and continued collecting data until just after the aircraft landed. After a flight was completed, the raw aircraft data were brought back to the ground station, where a program called `c3nav`¹ was used to compute the differential corrections to the aircraft positions and velocities.

The second problem with the GPS data was that the positions and velocities were limited to a 1 Hz sampling rate in Sessions 1 and 2, and to 10 Hz in Session 3 (Table 4). Additional data are required to fill the gap between the GPS sampling rate and the 40 Hz rate required for \mathbf{v}_p . This was supplied by the accelerometers on the probe. The raw 40 Hz data coming from the probe accelerometers are the acceleration vector $\hat{\mathbf{a}} = (\hat{a}_x, \hat{a}_y, \hat{a}_z)$ in the probe coordinate system. This vector is rotated into the (x, y, z) coordinate system using the roll, pitch, and yaw angles. The resulting rotated acceleration is $\mathbf{a} = (a_x, a_y, a_z)$.

After rotation of the accelerations, the GPS velocity measurements and \mathbf{a} are blended using an approach very similar to that used with the attitude angles. The GPS platform velocity \mathbf{v}_{pg} is assumed to be a low-frequency reference for \mathbf{v}_p , and the acceleration \mathbf{a} is assumed to be a high-frequency reference. Both vectors are Fourier transformed to frequency space. The acceleration is then time integrated by multiplying the Fourier transform $\mathbf{A}(f)$ of \mathbf{a} by the filter

$$G(f) = -\frac{i}{2\pi f}, \quad (7)$$

¹© M. Elizabeth Cannon and Gerard Lachapelle, University of Calagry, Canada

where i is equal to $\sqrt{-1}$. This integration converts \mathbf{A} into a Fourier-transformed velocity $\mathbf{V}_{\mathbf{pa}}(f)$. The accelerometer coefficients $\mathbf{V}_{\mathbf{pa}}$ are then blended with the GPS Fourier coefficients $\mathbf{V}_{\mathbf{pg}}(f)$ using the same method as described by Eqs. (4) and (5) for the attitude angles. After blending, the resulting Fourier coefficients $\mathbf{V}_{\mathbf{p}}(f)$ are inverse Fourier transformed to provide the 40 Hz probe velocity $\mathbf{v}_{\mathbf{p}}$.

5.3. Computation of $\mathbf{v}_{\mathbf{a}}$

The velocity $\mathbf{v}_{\mathbf{a}}$ of the air relative to the probe is computed from the pressure fluctuations measured at the probe. The front of the probe has a spherical shape, and the pressure distribution over this surface is given by (Brown et al. 1983; Crawford and Dobosy 1992)

$$p_{\xi} - p_s = q\left(1 - \frac{9}{4} \sin^2 \xi\right), \quad (8)$$

where q is the dynamic pressure, p_s is the static pressure, and p_{ξ} is the pressure at an angle ξ from the flow stagnation point on the sphere. (ξ is the angular separation as measured from the pressure sphere's center.) The probe is designed so that on average the stagnation point of the flow will be at port 0 (Fig. 3), but this point will move over the face of the probe as a result of variations in the relative wind vector $\hat{\mathbf{v}}_{\mathbf{a}}$. At any given time, the relative wind vector will form an angle with the probe \hat{x} axis, as shown in Fig. 9. The relative wind can have both an angle of attack α in the \hat{x} - \hat{z} plane (similar to latitude on the earth) and angle of sideslip β in the \hat{x} - \hat{y} plane (similar to longitude). Nonzero values of these angles will directly lead to displacements of the flow stagnation point away from port 0.

Given Eq. (8) and the measured pressures at the probe ports, the angles α and β can be computed. There is more than one way to do this, however. Leise and Masters (1991), for example, list three different derivations for these angles that they call the high-resolution, low-resolution, and NCAR methods. The main differences between the methods are what pressure measurements are available from the probe. The low-resolution method, which was used with the Long-EZ measurements prior to the MVP experiments, assumes that the dynamic pressure q and the differences $\delta\hat{p}_y$, and $\delta\hat{p}_z$ are available. The relative-wind angles can then be derived as (Leise and Masters 1991)

$$\tan \alpha = 2G_{\alpha} \left[1 + \sqrt{1 - 4(G_{\alpha}^2 + G_{\beta}^2)} \right]^{-1}; \quad (9)$$

$$\tan \beta = 2G_{\beta} \left[1 + \sqrt{1 - 4(G_{\alpha}^2 + G_{\beta}^2)} \right]^{-1}; \quad (10)$$

$$G_{\alpha} = \frac{2}{9} \left[\frac{\delta\hat{p}_z}{q} \right]; \quad (11)$$

$$G_{\beta} = \frac{2}{9} \left[\frac{\delta\hat{p}_y}{q} \right]. \quad (12)$$

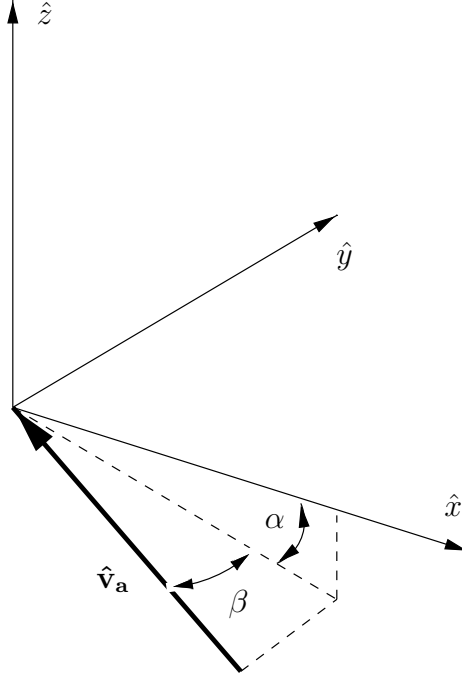


Figure 9: The angles α and β between the relative wind vector $\hat{\mathbf{v}}_{\mathbf{a}}$ and the probe \hat{x} axis.

One problem with these equations is that the Long-EZ probe measures the pressure difference $\delta\hat{p}_x$ rather than q . These quantities will be equal only when α and β are zero. The original approach was therefore to use an iterative approach in which $\delta\hat{p}_x$ was a first guess of q .

For the MVP postprocessing, the method used to estimate α and β was changed to what Leise and Masters (1991) called the NCAR method. This assumes from the outset that the available measurements are $\delta\hat{p}_x$, $\delta\hat{p}_y$, and $\delta\hat{p}_z$. The equations for α and β then become

$$\tan \alpha = 2H_\alpha \left[1 + \sqrt{1 + 5(H_\alpha^2 + H_\beta^2)} \right]^{-1}; \quad (13)$$

$$\tan \beta = 2H_\beta \left[1 + \sqrt{1 + 5(H_\alpha^2 + H_\beta^2)} \right]^{-1}; \quad (14)$$

$$H_\alpha = \frac{2\delta\hat{p}_z}{9\delta\hat{p}_x}; \quad (15)$$

$$H_\beta = \frac{2\delta\hat{p}_y}{9\delta\hat{p}_x}; \quad (16)$$

The advantage with these equations is that they do not contain the unknown variable q .

After the two angles are computed, this variable can be computed as

$$q = \delta \hat{p}_x \left[1 + \frac{9 (\tan^2 \alpha + \tan^2 \beta)}{4 - 5 (\tan^2 \alpha + \tan^2 \beta)} \right]. \quad (17)$$

When combined with a temperature measurement T (which can be either the probe or hatch temperature), the computed values of α , β , and q provide the information required to estimate the relative wind $\hat{\mathbf{v}}_{\mathbf{a}}$. The temperature must first be corrected for adiabatic heating resulting from the aircraft motion. The corrected temperature T' is related to the measured temperature T through the equation (Lenschow 1986; Leise and Masters 1991)

$$T' = T \left(1 + r \frac{\gamma - 1}{2} M^2 \right)^{-1}. \quad (18)$$

Here, $\gamma = c_{pm}/c_{vm}$ is the ratio of the specific heat c_{pm} at constant pressure for moist air to the corresponding specific heat c_{vm} at constant volume, M is the Mach number, and r is an empirical temperature recovery factor for the temperature probe. The Mach number is defined as

$$M^2 \equiv \frac{2}{\gamma - 1} \left[\left(1 + \frac{q}{p_s} \right)^{(\gamma-1)/\gamma} - 1 \right]. \quad (19)$$

The current processing software uses a modified version of Eq. (18) to compute the temperature correction. Since $q \ll p_s$ at the velocities flown by the Long-EZ, the Mach number can be estimated as

$$M^2 \approx \frac{2}{\gamma} \frac{q}{p_s}. \quad (20)$$

This is simply the first term in a Taylor series expansion of Eq. (19), and it is sufficiently accurate for use in the temperature correction. With Eq. (20), the temperature correction in Eq. (18) can be rewritten as a function of q and p_s :

$$T' = T \left(1 + r \frac{\gamma - 1}{\gamma} \frac{q}{p_s} \right)^{-1}. \quad (21)$$

The recovery factor r was set to 0.82 for the temperature sensors used in MVP.

The relative wind components can be obtained once the Mach number M and the corrected temperature T' are known. The probe's true air speed U_a is given by (Lenschow 1986; Leise and Masters 1991)

$$U_a = M \sqrt{\gamma R_m T'}, \quad (22)$$

with R_m representing the gas constant for moist air. [Note that the approximation in Eq. (20) is used only in the derivation of Eq. (21), not for computing M in Eq. (22)] The three components of the relative-wind vector $\hat{\mathbf{v}}_{\mathbf{a}}$ are then obtained from the equations

$$\hat{u}_a = -\frac{U_a}{\sqrt{1 + \tan^2 \alpha + \tan^2 \beta}}; \quad (23)$$

$$\hat{v}_a = -\hat{u}_a \tan \beta; \quad (24)$$

$$\hat{w}_a = -\hat{u}_a \tan \alpha. \quad (25)$$

The components from Eqs. (23)–(25) are still in the probe coordinate system shown in Fig. 3. These are rotated into earth coordinates using the attitude angles described in Section 5.1. This rotation produces the relative-wind vector \mathbf{v}_a . With \mathbf{v}_a computed from the equations in this section and \mathbf{v}_p from the foregoing section, the ambient wind \mathbf{v} is easily obtained from Eq. (1).

5.4. Processing of Scalar Quantities

The computation of the ambient wind vector \mathbf{v} is by far the largest fraction of the postprocessing effort. However, some of the other scalar variables sampled by the Long-EZ also require a limited amount of manipulation. As discussed in Section 3.4., the sensitivity and offset for the probe T_p and hatch T_h temperatures are recalibrated for each flight using the slow-response temperature T_b as a reference.

The IRGA measurements also required special treatment during postprocessing. This instrument provides fast-response measurements of the water-vapor density ρ_v and the CO₂ density ρ_c (Auble and Meyers 1992). A complicating factor in using the IRGA is that it has a nonlinear response to ρ_v . The response can be modeled as a quadratic function

$$\rho_v = c_2 V^2 + c_1 V + c_0, \quad (26)$$

with V representing output voltage. A further problem with the IRGA is that it suffers from baseline drift, so that a more appropriate version of the response function is

$$\rho_v = c_2 (V - V_o)^2 + c_1 (V - V_o) + c_0. \quad (27)$$

The variable V_o is a drift correction.

Since the drift correction is generally unknown, the IRGA is not suitable as a humidity reference. It is, however, capable of accurately measuring the higher frequency fluctuations of the humidity. This is done by considering the linear sensitivity $d\rho_v/dV$, which from Eq. (27) is

$$\frac{d\rho_v}{dV} = 2c_2(V - V_o) + c_1. \quad (28)$$

If Eq. (27) is solved for $V - V_o$, and the result is substituted into Eq. (28), the linear sensitivity becomes

$$\frac{d\rho_v}{dV} = \sqrt{c_1^2 - 4c_2(c_0 - \rho_v)}. \quad (29)$$

This shows that the linear sensitivity depends only on the known instrument constants and on the density ρ_v .

To use Eq. (29) in calibrating the IRGA, an independent measurement of ρ_v is required. This is obtained from the chilled mirror dew point T_d , which is easily converted to a slow-response estimate $\bar{\rho}_v$ of the water-vapor density. $\bar{\rho}_v$ is then substituted into Eq. (29) to

provide an estimate of $d\rho_v/dV$. The IRGA output is then assumed to follow the equation

$$\rho_v = \frac{d\rho_v}{dV}V + \rho_{vo} . \quad (30)$$

Here, ρ_{vo} is an arbitrary offset density, which will be constant as long as the baseline drift V_o is constant. This equation accounts for the IRGA nonlinearity in that $d\rho_v/dV$ is updated each second as a new value of T_d becomes available from the chilled mirror. Since the offset ρ_{vo} is arbitrary, Eq. (30) only provides the fluctuations of ρ_v about its mean value over time periods when ρ_{vo} is constant. For this reason, the IRGA is only used in computing the latent heat flux LE , which depends only on the fluctuations of ρ_v .

The drift V_o —and thus the offset ρ_{vo} —will remain constant as long as the aircraft does not fly through steep gradients of temperature and pressure. In practice, this means that the drift will remain constant as long as the aircraft flies at constant altitude. Hence, the IRGA ρ_v is typically used in the computation of latent heat fluxes over constant-altitude flight legs.

Another adjustment that was necessary for the hatch temperature and the IRGA measurements was a small shift in time to account for sensor location. These sensors are slightly downstream from the probe, and thus the observed fluctuations are slightly lagged relative to those on the probe. This lag is accounted for by shifting the hatch-temperature and IRGA time series slightly backward in time so that they are in phase with the probe measurements.

One other computation that is performed in postprocessing is the estimation of probe altitude Z_p using altimetry. This is done using a user-defined reference pressure p_{ref} , altitude Z_{ref} , and temperature T_{ref} (*e.g.*, Wallace and Hobbs 1977):

$$Z_p = \frac{T_{ref}}{\Gamma} \left[1 - \left(\frac{p_s}{p_{ref}} \right)^{R_d\Gamma/g} \right] + Z_{ref} . \quad (31)$$

The gas constant R_d for dry air, the gravitational acceleration g , and the ambient temperature lapse rate Γ appear in this equation. Γ was assumed to equal $9.8^\circ\text{C km}^{-1}$ during MVP, which should be reasonable within the convective boundary layer but less so in stable conditions. Generally, the reference values were obtained from the aircraft measurements during the time the aircraft was on the ground at the known airport elevation.

Aside from the variables discussed above, the other scalar variables did not require any significant manipulations in postprocessing.

5.5. Quality Control

A particularly time consuming aspect of the MVP Long-EZ data analysis was the development of software to identify and mark bad or suspect data. During the three MVP

sessions at Cape Canaveral, a variety of hardware and software problems caused noise in various data channels. Unfortunately, the noise often did not have highly distinctive features in either the time or frequency domains, so it was not always easy to identify and remove the noise.

5.5.1. GPS Positions and Velocities

The GPS positions and velocities were one common source of noise. As discussed previously, these data are collected digitally in the form of individual time-tagged messages. Some of the messages, however, became corrupted during some stage of the data acquisition. Sometimes the corruption was obvious, such as when the GPS measurements had the Long-EZ moving at supersonic speeds. Other times, this corruption was less obvious. Most of these corrupted GPS data were removed during postprocessing by applying a filtering program called `despike_gps` to the data. This program first tested the GPS data to ensure that each variable fell within user-specified minimum and maximum values. The aircraft’s horizontal speed, for example, was required to fall between 0 and 90 m s^{-1} , whereas the vertical speed was required to be in the range $\pm 8 \text{ m s}^{-1}$. If the measurement was outside the specified range, the measurement was rejected as bad.

Once a GPS variable was determined to fall within the specified range, `despike_gps` performed a second test on whether the rate of change of the variable was reasonable. The intention here was to detect and remove data spikes characterized by rapid variations within short periods of time. For each GPS variable b , a rate of change was defined as

$$\text{rate} = \frac{|b_i - b_{i-1}|}{(t_i - t_{i-1})}, \quad (32)$$

where b_i is the value at time t_i , and b_{i-1} is the value at an earlier time t_{i-1} . If this rate of change exceeded a user-specified value, the measurement was rejected as a spike. The maximum rates were determined by using data from individual flights to compute cumulative distribution functions for the rate of change of each GPS variable. These distribution functions tended to show a consistent behavior up to a certain rate, and then to become erratic at higher rates. It was assumed that the onset of the erratic behavior indicated where noise started to dominate the signal.

The algorithms in `despike_gps` removed a large fraction of the noise present in the GPS data. However, there still were less common cases involving lower-frequency contamination of the GPS velocities that went undetected by `despike_gps`. An attempt was made to identify these cases by comparing the GPS probe vertical velocity w_{pg} with an independent estimate of the vertical velocity obtained by differentiating the pressure altitude Z_p defined in Eq. (31). When the GPS was working correctly, the two vertical-velocity estimates were very similar. When the GPS velocity became corrupted, the two estimates deviated. (The Z_p measurement could, of course, also be corrupted, but this was much less frequent. Also, other parts of the postprocessing software tested the pressure measurements.) Once the two estimates deviated beyond a user-specified amount (usually 1 m s^{-1}), the GPS

velocities were rejected as bad. All three velocity components were rejected on the assumption that if the w_{pg} component is contaminated, there is a good chance that the u_{pg} and v_{pg} components are also contaminated.

5.5.2. System-Wide Noise

Another problem that was mainly a factor during MVP Session 2 was the simultaneous contamination of all the analog (*i.e.*, non GPS) channels by intermittent noise. There appeared to be some kind of electrical interference within the aircraft that was the source of the noise. One possible culprit was the aircraft radio transmitter. Although it was not proven definitively, there was a suspicion that the transmitter may have produced electrical noise whenever the pilot talked on the radio. Another possible source of the noise was transmission towers located near the flight legs of the Long-EZ. The reason this noise may have been more common during Session 2 was that the data acquisition system may not have been electrically shielded as well as in the other sessions.

The system-wide noise in the analog channels usually were shaped like “plateaus”. That is, the signal would first be fluctuating about one level, then would rapidly jump to a different level and stay there for a period before jumping back down to the original level. The width of the plateaus in time varied from just around one second up to about ten seconds. This noise structure is difficult to remove, because it is easy to see the plateaus by eye, but much harder to come up with a software algorithm that can reliably identify them.

Although the system-wide noise was present to some degree in all the analog channels, it was easiest to identify in the static pressure. A computer algorithm was therefore developed to identify the noise using this pressure. The pressure was first high-pass filtered to remove frequencies below about 0.05 Hz. Removal of these lower frequencies made the noise stand out better. The algorithm then searched for the noise plateaus by looking for their steep “edges”. The rate of change of the pressure at the edges of the plateaus was significantly larger in magnitude than the normal changes in pressure away from the noise. Hence, the algorithm searched along the filtered pressure signal until it found a location where the pressure’s rate of change exceeded a user-specified threshold. It was assumed that this location marked the front edge of a plateau. The algorithm then continued searching the signal for a second location having a rate of change exceeding the threshold, but this time the rate of change had to have the opposite sign of the first one. This location was assumed to be the back edge of the plateau. The entire plateau region was then marked in the software as being corrupted by noise.

Some refinements were added to the basic noise-detection algorithm described above. A maximum limit, for example, was placed on the width of a plateau in time. This was done in case the algorithm detected the front edge of a plateau but never found the back edge. Without a maximum limit, the algorithm could mark the entire remaining part of the flight as bad. The maximum limit was user-specified, and was generally set to 25 s. A visual inspection of the pressure signal before and after application of the algorithm indicated

that the algorithm did a credible job of identifying the noise without being overly conservative and incorrectly marking large regions of good data as being corrupted.

5.5.3. Quality Control on the Processed Data

A quality-control procedure was also applied to all the variables that were saved in the processed data. This procedure was similar to what was done with the raw GPS data. First, each variable was tested to see if it fell within user-specified minimum and maximum limits. Then, the rate of change of the variable with time was tested to see if it exceeded a maximum rate specified by the user. The intention of this latter test was to detect noise spikes that cause unrealistically rapid fluctuations in a variable. If the measurement failed either test, a flag was set to indicate that the data are suspect. The suspect data were still retained in the processed data in case other users disagreed with the quality-control procedures and wanted to use some of the flagged data.

5.6. Computer Programs

The postprocessing described in Sections 5.1. to 5.5. was performed in a series of programs written in the C/C++ programming languages. These programs started with the raw data described in Section 3.3. and upon completion created new files containing the processed data. The files with processed data are often referred to as POD (Processed Output Data) files to distinguish them from the raw files. The raw files are, of course, retained in case it is necessary or desired to reprocess the data.

The processing software makes extensive use of the NetCDF (Network Common Data Form) software developed by the University Corporation for Atmospheric Research/Unidata (Rew et al. 1997). NetCDF is a library of functions that allows users to store and retrieve data in a consistent manner that is machine independent. A big advantage of the library is that users can access the NetCDF data without having to know the details of the file's internal structure. The machine independence means that the data can be easily ported to other computer hardware and operating systems without software modifications. The library also has the ability to add metadata, such as variable units or text descriptions, to the NetCDF file. This allows the data to be self-contained in the sense that both the data and the information required to use the data are contained within the NetCDF file. The NetCDF library is provided as free software under a license that allows users to freely use, copy or modify the source code.

The postprocessing of the MVP data required 6 programs: `despike_gps`, `fixdgps`, `systemspike`, `adjust_cals`, `setref`, and `makepod`. These programs were run in the order listed. `despike_gps` scanned the GPS data for noise as described in Section 5.5.1. It created a new set of temporary files which contained the GPS data that remained after spike removal. For each GPS variable, `despike_gps` requires the user to specify a minimum and maximum value along with a threshold value for the variable's rate of change.

`fixdgps` was originally designed to synchronize the GPS data with the analog data channels and to fill in holes in the GPS data. In MVP Sessions 1 and 2, the GPS data stream was treated independently of the analog stream, so the two streams were not automatically synchronized in time. Time synchronization is accomplished in `fixdgps` by specifying a time lag between the GPS and analog signals. The program uses this lag to put the GPS data into its proper locations within the raw data file. Additionally, `fixdgps` used linear interpolation to fill in any missing GPS data. When a continuous stretch of missing data extended over only a short interval, the program interpolated without setting any data-quality flags. For larger intervals of missing data, the program still interpolated, but also set a flag indicating that interpolation over a long interval was required. The threshold interval length for setting the flag is user specified and depended on the sampling rate of the GPS data. For 10 Hz data, the threshold was typically a few seconds.

The proper time lag to use in `fixdgps` was computed in Sessions 1 and 2 by comparing the GPS pitch and roll measurements with the corresponding analog pitch and roll from the gyroscopes. The Fourier transforms of these signals were computed, and then the coherence and phase were separately computed between the two pitch measurements and between the two roll measurements. If the two signals are synchronized, the phase angle will be zero for all frequencies. If they are lagged by a time τ , the phase angle ζ will show a linear change with frequency having a slope equal to $2\pi\tau$. Hence, τ can be estimated by computing the slope of the phase angle.

For MVP Session 3, the aircraft data acquisition software synchronized the GPS data and the analog data in flight, so this task was not necessary in `fixdgps`. However, the program was still used in this session to interpolate over holes in the GPS data and to set a flag when a hole exceeded a specified size.

Another important task of `fixdgps` was to convert the raw data to the NetCDF file format. The raw data file (`mmddtttt.raw` or `mmddtttt.org` in Table 6) from the aircraft was in a nonportable binary format. `fixdgps` created a new NetCDF file with a `.ncr` extension. This file contained the same analog data as the `raw` or `org` file together with the synchronized and interpolated GPS data. All the programs following `fixdgps` used the `ncr` file rather than the `raw` or `org` file.

`systemspike` removed the noise affecting the analog channels as described in Section 5.5.2. When a region of corrupted data was detected, a flag was set to identify the region. All the analog channels were assumed to be corrupted when this kind of noise was detected.

`adjust_cals` was used to adjust the calibrations for the probe and hatch temperatures and on the IRGA. This procedure was described in Section 5.4.

`setref` was used to specify the reference pressure p_{ref} and reference altitude Z_{ref} required to compute the altitude as in Eq. (31). These were stored in the `ncr` file for later use by the `makepod` program.

`makepod` performed the bulk of the postprocessing, including the angle and wind computations described in Sections 5.1.–5.3. Starting with the `ncr` file, it created a new file with the file-name extension “.ncp”. This is the POD file containing the processed data. `makepod` also computed statistics on both the raw and processed data. These statistics are stored in a separate log file.

5.7. POD Files

The POD files are the final result of the postprocessing. They are NetCDF files containing time series of the ambient wind vector, temperature, humidity, and the other scalars measured by the aircraft. The contents of these files can be illustrated using the CDL (Common Data form Language) notation developed as part of the NetCDF software (Rew et al. 1997). CDL is a human-readable text notation that describes the contents of a NetCDF file. It has many similarities to the grammar of the C/C++ programming languages. The NetCDF software package comes with a utility called `ncdump` which can generate the CDL notation for any NetCDF file; this is an easy way to quickly scan the contents of the file.

An example of the CDL notation for one of the MVP POD files is given below.

```
netcdf 6122Lf1 {  
  
  dimensions:  
    Scan = UNLIMITED ; // (10043 currently)  
    Fast_scan = 40 ;  
  
  variables:  
    float Freq_slow ;  
      Freq_slow:long_name = "Sampling frequency of Scan" ;  
      Freq_slow:units = "hz" ;  
    float Freq_fast ;  
      Freq_fast:long_name = "Sampling frequency of Fast_scan" ;  
      Freq_fast:units = "hz" ;  
    int Stime ;  
      Stime:long_name = "File start time" ;  
      Stime:units = "seconds since 00:00:00 UTC" ;  
    short U(Scan, Fast_scan) ;  
      U:long_name = "East-west velocity component" ;  
      U:units = "meter second-1" ;  
      U:scale_factor = 0.001f ;  
      U:add_offset = 0.f ;  
    short V(Scan, Fast_scan) ;  
      V:long_name = "North-south velocity component" ;
```

```

    V:units = "meter second-1" ;
    V:scale_factor = 0.001f ;
    V:add_offset = 0.f ;
short W(Scan, Fast_scan) ;
    W:long_name = "Vertical velocity component" ;
    W:units = "meter second-1" ;
    W:scale_factor = 0.0005f ;
    W:add_offset = 0.f ;
short Tp(Scan, Fast_scan) ;
    Tp:long_name = "Probe Temperature" ;
    Tp:units = "kelvin" ;
    Tp:scale_factor = 0.001f ;
    Tp:add_offset = 294.6188f ;
short Th(Scan, Fast_scan) ;
    Th:long_name = "Hatch temperature" ;
    Th:units = "kelvin" ;
    Th:scale_factor = 0.001f ;
    Th:add_offset = 294.9907f ;
short RhoD(Scan, Fast_scan) ;
    RhoD:long_name = "Dry air density" ;
    RhoD:units = "kilogram meter-3" ;
    RhoD:scale_factor = 1.e-04f ;
    RhoD:add_offset = 0.f ;
short F_CO2(Scan, Fast_scan) ;
    F_CO2:long_name = "IRGA CO_2 concentration" ;
    F_CO2:units = "milligram meter-3" ;
    F_CO2:scale_factor = 0.0122f ;
    F_CO2:add_offset = 420.3667f ;
short F_H2O(Scan, Fast_scan) ;
    F_H2O:long_name = "IRGA H_2O concentration" ;
    F_H2O:units = "gram meter-3" ;
    F_H2O:scale_factor = 0.001276145f ;
    F_H2O:add_offset = 36.4476f ;
short Ps(Scan, Fast_scan) ;
    Ps:long_name = "Static pressure" ;
    Ps:units = "millibar" ;
    Ps:scale_factor = 0.001210085f ;
    Ps:add_offset = 998.1371f ;
int Lat(Scan) ;
    Lat:long_name = "Latitude" ;
    Lat:units = "deg" ;
    Lat:scale_factor = 3.05e-05f ;
    Lat:add_offset = 28.5f ;
int Lon(Scan) ;
    Lon:long_name = "Longitude" ;

```

```

    Lon:units = "deg" ;
    Lon:scale_factor = 3.05e-05f ;
    Lon:add_offset = -80.5f ;
short Alt(Scan) ;
    Alt:long_name = "Altitude" ;
    Alt:units = "meter" ;
    Alt:scale_factor = 0.25f ;
    Alt:add_offset = 0.f ;
short PARU(Scan) ;
    PARU:long_name = "Upward PAR" ;
    PARU:units = "micromole meter-2 second-1" ;
    PARU:scale_factor = 0.1277589f ;
    PARU:add_offset = -5.11306f ;
short PARD(Scan) ;
    PARD:long_name = "Downward PAR" ;
    PARD:units = "micromole meter-2 second-1" ;
    PARD:scale_factor = 0.10289f ;
    PARD:add_offset = 2.2636f ;
short NetR(Scan) ;
    NetR:long_name = "Net Radiation" ;
    NetR:units = "watt meter-2" ;
    NetR:scale_factor = 0.0302651f ;
    NetR:add_offset = 482.742f ;
short SfcT(Scan) ;
    SfcT:long_name = "Surface Temperature" ;
    SfcT:units = "kelvin" ;
    SfcT:scale_factor = 0.009407f ;
    SfcT:add_offset = 271.8207f ;
short S_CO2(Scan) ;
    S_CO2:long_name = "Licor CO_2 concentration" ;
    S_CO2:units = "micromole mole-1" ;
    S_CO2:scale_factor = 0.0081f ;
    S_CO2:add_offset = 350.f ;
short Tdew(Scan) ;
    Tdew:long_name = "Dew point" ;
    Tdew:units = "Celsius" ;
    Tdew:scale_factor = 0.0028f ;
    Tdew:add_offset = 6.2363f ;
short AirSpd(Scan) ;
    AirSpd:long_name = "Aircraft speed" ;
    AirSpd:units = "meter second-1" ;
    AirSpd:scale_factor = 0.00375f ;
    AirSpd:add_offset = 50.f ;
int Dataflag(Scan, Fast_scan) ;
    Dataflag:long_name = "Data quality flag" ;

```

```
Dataflag:bit_settings = "..." ;
```

The top line in the CDL notation indicates that this is NetCDF file “6122Lf1”. The `ncp` file extension has been left off in the notation, so the actual file name is “6122Lf1.ncp”. This file-name convention differs from that described in Section 3.3. That section described the `mmddtttt` convention used in the data acquisition software. However, the MVP program established its own file-name convention. For the Long-EZ data, this convention is “ydddLfn”, where `y` is the year (5=1995, 6=1996), `ddd` is the Julian day, `L` indicates the file contains Long-EZ data, and `f` indicates the following number `n` is the flight number on a particular day (counting up from 1). In the CDL example above, the file contains data from flight 1 on day 122, 1996.

After the file name, the CDL text describes the array dimensions that are present in the file. In the POD file, there are two dimensions: `Scan` and `Fast_scan`. `Scan` is a time dimension representing one-second intervals in the data. In the example, the length of the `Scan` dimension is 10043. This particular flight therefore lasted about 2 hours and 47 minutes. Each index value in the `Scan` dimension represents one second of data. The `Fast_scan` dimension is used to subdivide the one-second scans. For MVP, this dimension always has a length of 40, because this matches the 40 Hz sampling frequency of the fast data channels. Each index in `Fast_scan` represents one of the 40 data values sampled within one second.

After the dimensions, the CDL notation above lists all the variables present in the NetCDF file. These variable listings are generally self explanatory. Each variable is either a `float` (4-byte floating point number), an `int` (4-byte integer), or `short` (2-byte integer). The variable can also be a scalar (*e.g.*, `Freq_slow`), a one-dimensional array [*e.g.*, `Lat(Scan)`], or a two-dimensional array [*e.g.*, `U(Scan,Fast_scan)`]. The one-dimensional variables are the slow data that are archived once per second. The two-dimensional variables are the 40 Hz fast data. With these variables, `Fast_scan` varies the fastest in memory.

Each variable can also have attributes attached to it. These are listed in the CDL notation on lines after the variable name. The `long_name` and `units` attributes are self explanatory. The `scale_factor` and `add_offset` attributes are used to convert integer data values to the units specified by the `units` attribute. To save storage space, most of the data are stored as 2-byte `short` integers. To obtain a floating-point value in the proper `units`, this integer is first multiplied by the `scale_factor`; the result is then added to the `add_offset`.

The `Data_flag` variable is different in that it contains the flags set during the various quality-control checks in the processing software. Each bit in this variable is a flag having a specific meaning regarding data quality. A flag is set when the bit is 1 and is unset when the bit is 0. Table 12 lists all the flags contained within `Data_flag`. Most simply indicate that a particular data channel is bad. `UVWgap`, `Latgap`, and `Longap` indicate that a GPS data value has been interpolated over a long gap. The threshold gap length used in setting this flag is specified as input to the `fixdgps` program. The `Nodiffcor` flag is set when

Table 12: Data quality flags used with the `Data_flag` variable in the processed aircraft data. The standard C-language convention is used, in that hexadecimal values are prepended with “0x”.

Name	Hexadecimal value	Meaning
UVbad	0x1	Bad horizontal velocity
Wbad	0x2	Bad vertical velocity
Tpbad	0x4	Bad probe temperature
Thbad	0x8	Bad hatch temperature
FCO2bad	0x10	Bad IRGA CO ₂
FH2Obad	0x20	Bad IRGA H ₂ O
Psbad	0x40	Bad static pressure
Latbad	0x80	Bad latitude
Lonbad	0x100	Bad longitude
Altbad	0x200	Bad altitude
PARUbad	0x400	Bad PAR up
PARDbad	0x800	Bad PAR down
Netbad	0x1000	Bad net radiation
SfcTbad	0x2000	Bad surface temperature
SCO2bad	0x4000	Bad Licor CO ₂
Tdewbad	0x8000	Bad dew point
Spdbad	0x10000	Bad air speed
UVWgap	0x20000	Long gap in GPS velocity
Latgap	0x40000	Long gap in GPS Latitude
Longap	0x80000	Long gap in GPS Longitude
Nodiffcor	0x100000	No GPS differential corrections

differential corrections were not available for the GPS data. A total of 21 flags are listed in Table 12, so the remaining 10 bits (excluding the sign bit) are currently unused.

5.8. Utility Programs

Several utility programs are available for obtaining information from the POD files. The `ncdump` program, which comes with the NetCDF software, has already been mentioned. It lists the contents of a NetCDF file to standard output using the CDL notation. This program is useful for getting a quick view of the file contents.

Other utilities have been developed as part of the MVP software development. The `extract` program was developed to extract data from a NetCDF file and send it in ascii format to standard output, where it can be redirected to a file or piped to another process. It prints the data as a simple column of numbers so that they can be used by other

programs that do not read NetCDF files directly. The `flagstats` utility displays a table of the frequencies at which the various data flags are set. It requires as input the name of the POD file together with a start scan and end scan. The output lists the percentage of the time the flags are set within the specified range of scans.

One of the more important utilities is `makestats`. It is used to generate statistics on the POD data. These statistics include the mean speed and direction, mean temperature and specific humidity, velocity standard deviations, and the sensible and latent heat fluxes. The statistics are organized according to the marker file that is supplied along with the POD file. A separate set of statistics is generated for each marker pair. The original marker file that was used during the data processing can be used if desired with `makestats`, but alternative or modified marker files can be used if this is useful for a specific investigation. `makestats` also requires the user to specify the number of one-second scans to be used in running averages. This affects the range of scales that are included in the flux and turbulence statistics.

6. Data Collected in Sessions 1–3

The Long-EZ aircraft measurements were designed to support the overall MVP field effort during the three Cape Canaveral sessions. Hence, the number of flights flown in each session partly depended on how often the SF₆ tracer was released. Other important factors were the weather, hardware malfunctions, and limitations placed by operational activities (*e.g.*, rocket launches) at the Cape. This section provides an overview of the Long-EZ flights that took place during each session.

6.1. Session 1

This session officially took place from 5 July to 2 August 1995. However, a series of operational and hardware problems delayed the start of the tracer releases. The first tracer release occurred on 18 July, and the last occurred on 31 July. Although the Long-EZ normally was intended to fly during tracer releases, it was decided to start taking measurements prior to the start of the tracer releases on 18 July. Some short calibration flights were flown on 8 and 12 July. The first data-collection flight was on 13 July, and the last was on 28 July.

The aircraft was plagued by a series of hardware problems during this session. A major factor appears to have been that Session 1 was at the end of a heavy schedule of experiments involving the Long-EZ during the summer of 1995. Some of the hardware simply started to wear out by the MVP experiment. The gyroscopes were a frequent source of trouble. A more serious problem was the loss of the $\delta\hat{p}_y$ sensor early in the session. The data from this sensor looked reasonable during the experiment, but it was not discovered until the postprocessing that the data were corrupted. This basically led to the loss of

Table 13: Long-EZ flights during MVP Session 1. The start time and duration represent the period when data were collected. The abbreviations in the Patterns column are SB for sea breeze, F for flux, OF for ocean flux, BP for box pattern, and SA for spiral ascent. These are described in Section 4.1. The multifile column indicates whether the flight data are in one POD file or multiple files.

Date	Start Time (EST)	Duration (hr:min)	File name	Altitudes (m)	Patterns	Multi-file
7/13/95	1458	1:42	5194Lf1	166–1508	SB	n
7/15/95	1520	3:03	5196Lf1	134–1552	SB, F	y
7/18/95	1110	0:52	5199Lf1	170	SB	n
7/18/95	1559	0:50	5199Lf2	176–204	SB	n
7/23/95	1025	3:32	5204Lf1	37–1560	OF, SB, SA	y
7/23/95	1821	1:32	5204Lf2	150–1500	SA, BP	y
7/24/95	1240	1:30	5205Lf1	53–185	OF, SB	n
7/25/95	1150	1:39	5206Lf1	182–975	BP, SB	y
7/26/95	0934	2:22	5207Lf1	69–1554	BP, SB, OF	y
7/27/98	0911	2:28	5208Lf1	22–189	BP, F	y
7/28/98	0924	0:39	5209Lf1	502	BP	y

much of the wind measurements during the session.

Table 13 lists the 11 Long-EZ data flights conducted during Session 1. For the entire session about 20 hours of aircraft data were collected. The patterns mentioned in Table 13 are described in Section 4.1. The sea-breeze pattern represents the flight legs shown in Fig. 4. Ideally, the data for an entire flight would be contained in a single POD file. However, the data acquisition system sometimes failed and was restarted in flight. Some flights therefore have more than one POD file. These flights are shown in Table 13 with a “y” in the multifile column.

Table 14 is a summary of the data-quality flags in the Session 1 data. It lists the percentage of unflagged scans for selected variables from each flight. This can be interpreted as a data recovery rate. After the two first flights, no good velocity data are available primarily because of a failure in the $\delta\hat{p}_y$ sensor. The probe temperature sensor also malfunctioned at the same time, but the hatch temperature is available as a substitute. The other sensors tend to have recovery rates similar to the last three columns in Table 14.

6.2. Session 2

MVP Session 2 took place from 28 October to 19 November 1995. Tracer releases occurred between 1 and 18 November. The Long-EZ collected data between 1 and 16 November.

Table 14: Summary of the data quality for selected variables in the Session 1 flights.

Flight	Unflagged data (%)					
	Horizontal velocity	Vertical velocity	Probe temperature	Hatch temperature	IRGA H ₂ O	Static pressure
5194Lf1	100	100	97	100	100	100
5196Lf1	97	97	96	100	100	100
5199Lf1	0	0	0	99	99	99
5199Lf2	0	0	0	98	98	98
5204Lf1	0	0	0	99	99	99
5204Lf2	0	0	0	100	100	100
5205Lf1	0	0	0	93	93	93
5206Lf1	0	0	0	90	90	90
5207Lf1	0	0	0	93	93	93
5208Lf1	0	0	0	97	97	97
5209Lf1	0	0	0	100	100	100

Overall, both the experiment as a whole and the Long-EZ flights in particular went considerably more smoothly in Session 2 than in Session 1. A large quantity of data was collected during the session. The only significant problem that arose during this session was the appearance of the system noise described in Section 5.5.2. Because of this noise, the `systemspike` program was added to the list of postprocessing programs. The noise was far less significant in the other two sessions, so it appears that it was due to some hardware configuration specific to Session 2.

Table 15 summarizes the Session 2 Long-EZ flights. In total about 81 hours of data were collected. Most of the data were collected along the three legs shown in Fig. 6. The data acquisition system worked reliably during this session, so only one flight in Table 15 had a system failure that required a restart (and thus creating multiple POD files) during the flight.

Table 16 provides information on the data recovery rate for Session 2. The hatch temperature sensor failed after the first three flights, but this is really only a backup for the probe temperature, which worked throughout the session. The velocity components have lower recovery rates than the other variables. This is mostly due to problems with the GPS data. Most of the data loss indicated for the nonvelocity variables in Table 16 is due to the system-wide noise discussed in Section 5.5.2.

Table 15: Long-EZ flights during MVP Session 2. The columns have the same meaning as in Table 13. For the patterns, TJ, SN, and GX are the three flight legs in Fig. 6, and OF is ocean flux.

Date	Start Time (EST)	Duration (hr:min)	File name	Altitudes (m)	Patterns	Multi-file
11/1/95	0947	3:35	5305Lf1	18–1700	TJ,SN,GX,OF	n
11/1/95	1448	2:52	5305Lf2	18–1668	TJ,SN,GX,OF	n
11/2/95	1043	2:45	5306Lf1	25–1674	TJ,GX,OF	n
11/2/95	1425	3:07	5306Lf2	17–1678	TJ,SN,GX,OF	n
11/3/95	0701	1:31	5307Lf1	13–289	GX,OF	n
11/3/95	1105	3:08	5307Lf2	28–1668	GX,SN,TJ	n
11/5/95	1008	3:33	5309Lf1	28–1693	TJ,SN,GX,OF	n
11/5/95	1424	1:44	5309Lf2	62–1658	TJ	n
11/6/95	1011	3:34	5310Lf1	21–1843	TJ,SN,GX,OF	n
11/6/95	1554	3:10	5310Lf2	37–1671	TJ,SN,GX	n
11/7/95	0945	3:04	5311Lf1	52–1690	GX,SN,TJ	n
11/7/95	1459	3:21	5311Lf2	32–1694	TJ,GX,OF	n
11/8/95	0823	2:31	5312Lf1	61–1255	TJ	n
11/8/95	1148	4:29	5312Lf2	25–1685	GX,SN,TJ	n
11/9/95	0904	3:33	5313Lf1	36–1645	GX,SN,TJ	n
11/9/95	1416	2:49	5313Lf2	43–1658	GX,SN,TJ	n
11/10/95	1139	3:26	5314Lf1	53–1648	TJ,SN,GX	n
11/11/95	1215	4:14	5315Lf1	32–1669	TJ,GX	y
11/13/95	1328	3:20	5317Lf1	41–1660	TJ,GX,OF	n
11/13/95	1931	3:04	5317Lf2	58–322	TJ,SN	n
11/14/95	1244	3:55	5318Lf1	50–1643	GX,TJ	n
11/14/95	1829	4:11	5318Lf2	67–335	TJ,SN	n
11/15/95	1301	4:56	5319Lf1	32–1643	TJ,SN,GX,OF	n
11/16/95	0701	2:18	5320Lf1	37–346	TJ	n
11/16/95	1154	2:35	5320Lf2	53–1630	TJ	n

Table 16: Summary of the data quality for selected variables in the Session 2 flights.

	Unflagged data (%)					
Flight	Horizontal velocity	Vertical velocity	Probe temperature	Hatch temperature	IRGA H ₂ O	Static pressure
5305Lf1	76	76	91	91	91	91
5305Lf2	91	91	94	94	94	94
5306Lf1	81	81	97	97	97	97
5306Lf2	84	84	94	0	94	94
5307Lf1	84	85	98	0	98	98
5307Lf2	84	84	97	0	97	97
5309Lf1	91	91	93	0	93	93
5309Lf2	98	98	100	0	100	100
5310Lf1	91	91	95	0	95	95
5310Lf2	92	92	95	0	95	95
5311Lf1	83	83	93	0	93	92
5311Lf2	94	94	98	0	98	98
5312Lf1	87	87	90	0	90	90
5312Lf2	88	88	98	0	98	98
5313Lf1	94	94	96	0	96	96
5313Lf2	94	94	99	0	99	99
5314Lf1	95	95	99	0	99	99
5315Lf1	96	96	99	0	99	99
5317Lf1	91	91	96	0	96	95
5317Lf2	84	84	88	0	88	88
5318Lf1	92	92	95	0	95	95
5318Lf2	84	86	97	0	97	97
5319Lf1	93	93	96	0	96	96
5320Lf1	96	96	98	0	98	98
5320Lf2	83	83	86	0	86	86

Table 17: Long-EZ flights during MVP Session 3. The columns have the same meaning as in Table 13. For the patterns, TJ, UN, and DE are the three flight legs in Fig. 7, CZ is the convergence-zone pattern in Fig. 8, and OF is ocean flux.

Date	Start Time (EST)	Duration (hr:min)	File name	Altitudes (m)	Patterns	Multi-file
4/26/96	1349	0:32	6117Lf1	38–174	UN	n
4/27/96	1718	2:59	6118Lf1	39–1684	UN,TJ	y
4/28/96	1019	1:36	6119Lf1	46–1709	UN	n
4/28/96	1519	3:04	6119Lf2	31–1664	TJ,DE	n
4/29/96	0752	4:43	6120Lf1	26–1657	UN,TJ,DE	n
4/29/96	1413	3:37	6120Lf2	41–1671	TJ,DE	n
5/1/96	0451	2:47	6122Lf1	35–326	TJ,UN	n
5/1/96	1004	3:32	6122Lf2	39–1663	TJ,DE,OF	n
5/2/96	0405	2:04	6123Lf1	48–419	CZ	n
5/2/96	0935	3:11	6123Lf2	45–1665	CZ	n
5/2/96	1346	2:27	6123Lf3	31–1658	CZ	n
5/3/96	0923	3:40	6124Lf1	47–1655	CZ,UN,TJ	n
5/3/96	1348	2:39	6124Lf2	32–1674	UN,TJ,DE	n
5/4/96	0710	3:32	6125Lf1	36–546	CZ,UN	n
5/4/96	1357	2:43	6125Lf2	44–1673	TJ,DE	n
5/5/96	0947	3:18	6126Lf1	45–1655	CZ	y
5/5/96	1744	2:56	6126Lf2	40–937	UN,TJ	n
5/6/96	1842	3:16	6127Lf1	53–941	TJ,UN	n
5/7/96	1054	3:51	6128Lf1	30–1689	CZ,UN,TJ,DE	n
5/9/96	0540	3:45	6130Lf1	30–949	UN,TJ,DE	n
5/9/96	1000	3:53	6130Lf2	42–1665	UN,TJ,DE	n

6.3. Session 3

Session 3 occurred in late April and May 1996. The first Long-EZ flight took place on 26 April, and the last was on 9 May. As with Session 2, the data acquisition system worked reliably during this session, so the quantity and quality of the measurements met or exceeded expectations.

Table 17 provides a summary of the Long-EZ data collection during Session 3. Twenty-one flights were conducted, providing about 64 hours of data. Only two flights in Table 17 had a system failure that resulted in the creation of multiple POD files. Most of the flights concentrated on the earlier part of the day; there were 5 during the early morning, 7 during late morning, 5 during early afternoon, 3 during late afternoon, and just one in the evening.

Table 18: Summary of the data quality for selected variables in the Session 3 flights.

Flight	Unflagged data (%)					
	Horizontal velocity	Vertical velocity	Probe temperature	Hatch temperature	IRGA H ₂ O	Static pressure
6117Lf1	96	96	100	100	100	100
6118Lf1	98	98	100	100	100	100
6119Lf1	96	96	100	100	100	100
6119Lf2	94	94	99	99	99	98
6120Lf1	99	99	100	100	100	100
6120Lf2	98	98	100	100	0	99
6122Lf1	98	98	100	100	0	100
6122Lf2	95	95	100	100	100	99
6123Lf1	94	94	100	100	100	100
6123Lf2	96	96	100	100	100	99
6123Lf3	96	96	100	100	100	100
6124Lf1	97	97	100	100	100	99
6124Lf2	98	98	100	100	100	100
6125Lf1	99	99	100	100	100	100
6125Lf2	95	95	100	100	100	99
6126Lf1	96	96	100	100	100	99
6126Lf2	99	99	100	100	100	100
6127Lf1	99	99	100	100	100	100
6128Lf1	96	96	100	100	100	99
6130Lf1	98	98	100	100	100	100
6130Lf2	92	93	100	100	100	99

A summary of the data recovery rates is provided in Table 18. These recovery rates remained high throughout the session. Compared with Session 2, the difference in recovery rates between the velocity and the other variables is not as large in Session 3. The IRGA sensor failed on the second flight on day 120, but it was replaced in time for the second flight on day 122.

Overall, there was a steady improvement in the performance of the Long-EZ data acquisition system over the course of the three MVP Sessions at Cape Canaveral. Several significant problems were encountered during Session 1, which led to a low data recovery rate for the velocities. In Session 2, the performance improved significantly, with over half of the flights having velocity recovery rates above 90% and all but one having recovery rates above 80%. In Session 3, all the velocity recovery rates were above 90%.

7. Selected Results

This report is primarily intended to describe the collection and postprocessing of the Long-EZ data from MVP Sessions 1–3. It is not intended to provide a detailed scientific analysis of the data. However, a few selected examples are provided in this section to indicate the kinds of information that can be extracted from the data.

MVP Session 1 focused on the horizontal structure of the sea breezes. Most of the data collected during this session were therefore collected while flying legs perpendicular to the coast, as shown in Fig. 4. Figure 10 is an example of the data collected along the C–A leg during the afternoon of 13 July 1995. The solid lines represent data collected along the C–A leg while the aircraft was flying at about 170 m MSL. The dashed lines represent a return leg between Z and C at 1590 m MSL.

From the observed wind directions at the higher altitude, it is clear that the prevailing synoptic flow was between the east and southeast during this period. The synoptic flow was therefore onshore during this flight. Previous studies (*e.g.*, Arritt 1993; Atkins and Wakimoto 1997) have indicated that onshore synoptic flows tend to suppress the development of sea breezes. However, there is evidence in Fig. 10 that a sea breeze enhanced the low-level onshore flow near the coast. The 170 m wind speed, for example, starts out at about 2 m s^{-1} at the greatest distances offshore and then steadily increases to about 6 m s^{-1} just inland from the coast. It then steadily decreases to about 4 m s^{-1} at 30 km inland. Throughout this range the 1590 m wind speed is less than the 170 m speed. This suggests that a sea-breeze circulation is enhancing the lower-level winds.

The potential-temperature measurements in Fig. 10 also support the presence of a sea-breeze enhancement of the winds. Over the water the 170 m potential temperature remains relatively steady at about 300 K. Inland, the temperature steadily rises by about 1.5 K. The turbulent kinetic energy at 170 m rapidly increases between the coast and 30 km inland, but then decreases further inland. One possible explanation for this is that the sea-breeze front was located about 30–40 km inland at the time of the measurements.

Overall, Fig. 10 suggests that a sea-breeze circulation may have influenced the winds between about 30–40 km offshore and about the same distance inland. Aircraft data such as these, together with measurements from fixed instruments and remote sensors, will be useful in determining the importance and spatial structure of the sea breezes at Cape Canaveral.

During Sessions 2 and 3, more emphasis was placed on the vertical flow structure. The horizontal lengths of the flight legs were reduced (*e.g.*, Figs. 6 and 7) to allow more time for flying multiple altitudes. Figure 11 shows examples of early morning profiles taken over land on 16 November 1995. The aircraft first flew the T–J leg at altitudes from 40 to 350 m MSL during the hour from 0700–0800 EST, and then repeated the same pattern about an hour later.

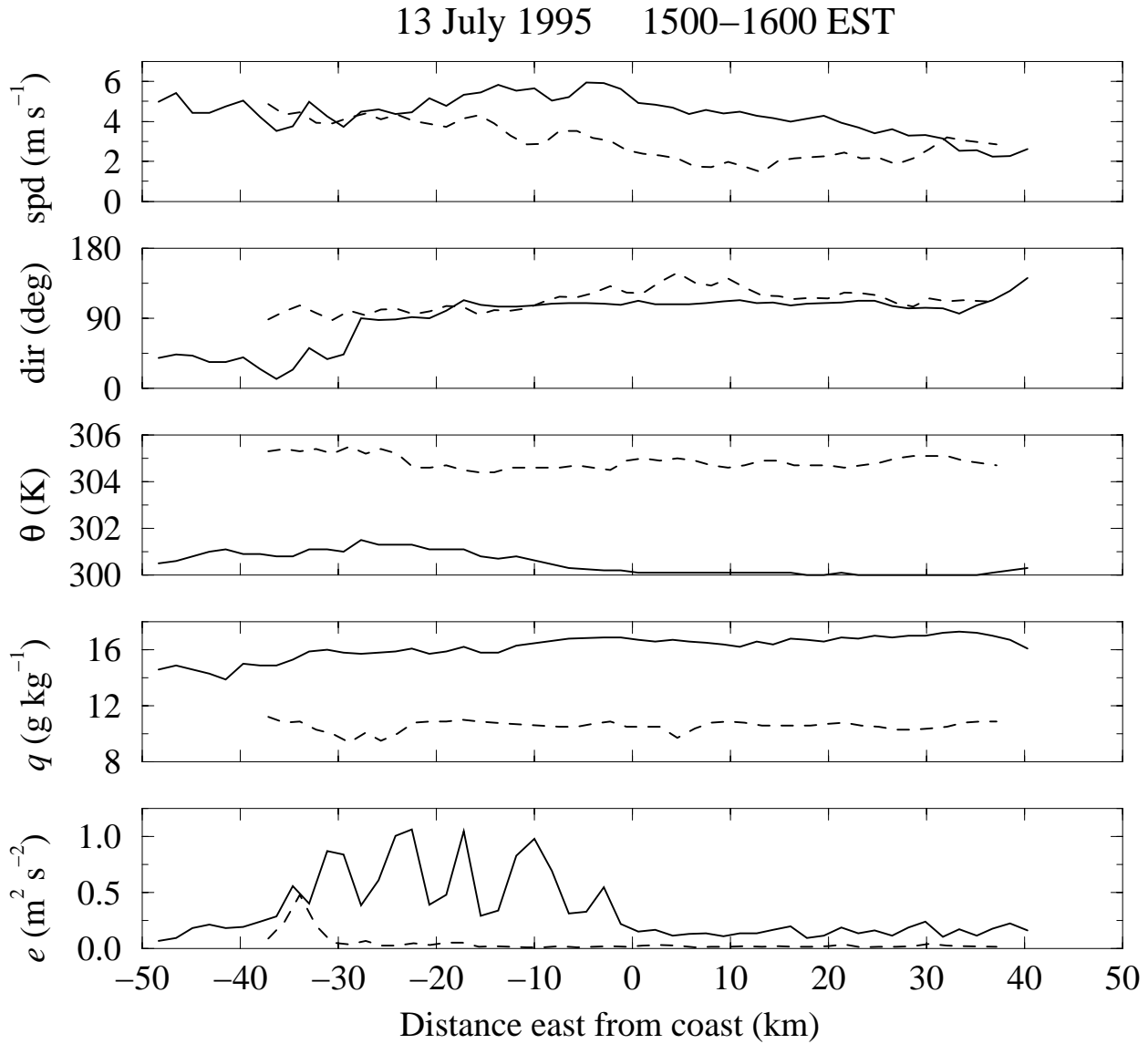


Figure 10: Plots of wind speed (spd) and direction (dir), potential temperature (θ), specific humidity (q), and turbulent kinetic energy (e) for a Long-EZ flight on 13 July 1995. The solid lines are for a C–A (see Fig. 4) leg at 170 m MSL, and the dashed lines are a Z–C leg at 1590 m MSL. All the variables are computed using 30 s running averages.

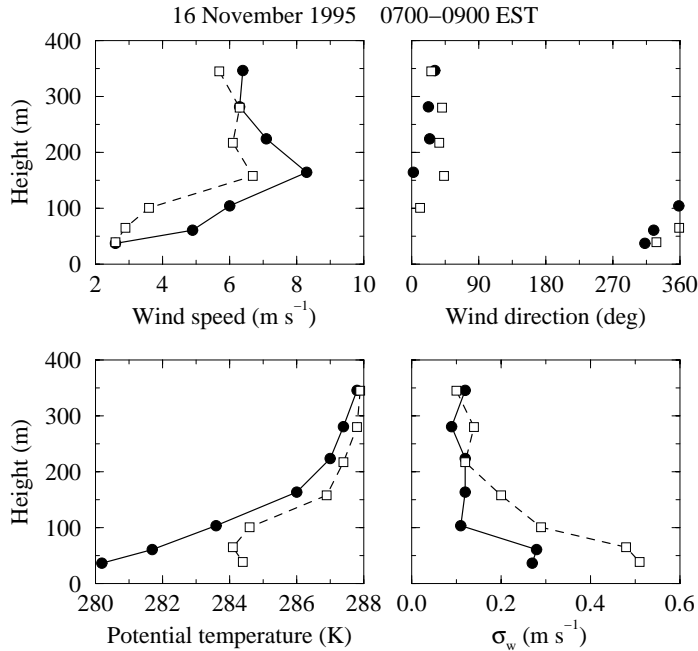


Figure 11: Profiles of wind speed and direction, potential temperature, and σ_w for the morning of 16 November 1995. The solid lines and filled circles are for the 0700–0800 EST time period, and the dashed lines and open squares are for the 0800–0900 EST period.

The 0700 EST potential-temperature profile in Fig. 11 clearly shows the presence of a stable boundary layer. The surface inversion appears to extend up to roughly 350 m. A low-level jet is present at about 150 m. This jet appears to be associated with a shift in wind direction from northwesterly below to northeasterly aloft. The vertical velocity fluctuations σ_w reach about 0.3 m s^{-1} near the ground, but rapidly fall off to about 0.1 m s^{-1} above 50 m.

By the 0800 EST profile, the solar heating has eroded the first 50–100 m of the surface inversion. The heating has also roughly doubled σ_w near the surface. However, the wind direction has changed little, and the wind speed has decreased at most levels. Figure 11 demonstrates how the Long-EZ can be used to provide useful profiles of both mean and turbulence quantities throughout the depth of the boundary layer.

The last example discussed here demonstrates the large differences in boundary-layer structure that can exist between the land and sea near Cape Canaveral. Figure 12 shows vertical profiles taken during the afternoon on 4 May 1996 (MVP Session 3). The aircraft flew the land T–J leg (Fig. 7) between about 1420 and 1500 EST and then flew the sea E–D leg about an hour later.

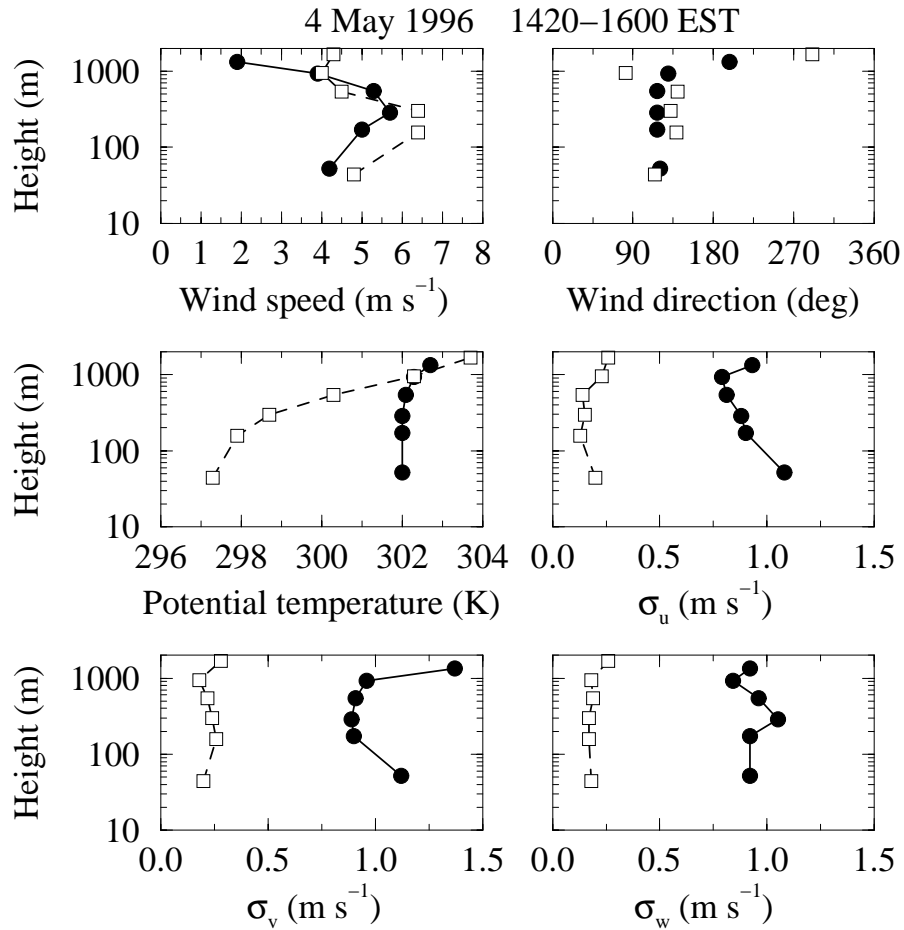


Figure 12: Profiles of wind speed and direction, potential temperature, and the three velocity standard deviations σ_u , σ_v , and σ_w for the afternoon of 4 May 1996. The solid lines and filled circles are for the T–J leg over land, and the dashed lines and open squares are for the E–D leg over the ocean. The T–J data were collected between 1420 and 1500 EST, whereas the E–D data were collected between 1520 and 1600 EST.

The mean winds along the two legs were not all that different, although the sea leg has somewhat higher wind speeds below about 300 m. The potential temperature, however, indicates that a well-mixed convective boundary layer having a depth of roughly 1000 m existed over the land, whereas over the sea the boundary layer was near-neutral to slightly stable and only had a depth of about 200 m. The velocity standard deviations show dramatic differences between the two legs; they are about four times larger over the land than over the sea. It is also interesting to note that the standard deviations—particularly σ_v —tend to increase above about 1000 m. This may be the result of turbulence generated by the wind-shear layer that exists at this level.

Measurements of land-sea differences such as Fig. 12 will be useful for improving the dispersion models used at Cape Canaveral. The models currently in use, such as REEDM (Bjorklund 1990), use a single turbulence estimate for the entire region surrounding the launch pads at the Cape. In situations such as Fig. 12, this is clearly inaccurate. The situation becomes even more complicated when considering that the launch pads are in the transition zone between the maritime boundary layer seen at the E–D leg and the land boundary layer observed at T–J.

8. Summary

The NOAA Long-EZ aircraft participated in all three of the MVP Sessions at Cape Canaveral. About 165 hours of data were collected during these sessions. Hardware problems, weather cancellations, and administrative delays plagued Session 1, but the Long-EZ deployments during Sessions 2 and 3 were highly successful. The total flight hours for these two sessions met or exceeded expectations, and the data are of high quality.

During MVP, many improvements were made to the software used to process the raw aircraft data. These improvements were necessary partly because the use of the Long-EZ during MVP was somewhat different than during previous deployments of the aircraft. Many other improvements were made that will benefit future processing of Long-EZ data, including the data from the May 1997 MVP experiment at Vandenberg Air Force Base, California. These improvements include the use of the NetCDF library for machine-independent data storage, the use of enhanced filtering techniques based on Fast Fourier Transforms, and the inclusion of a data quality flag in the processed data.

The Long-EZ data are an important component of the overall MVP field effort. It was one of the few measurement platforms that could provide turbulence measurements aloft at altitudes where the rocket exhaust clouds typically stabilize after their buoyant rise. Its mobility allowed it to collect measurements over a variety of surface types (land, sea, rivers) within a short period of time. The aircraft measurements will be highly useful for evaluating both the current operational dispersion models such as REEDM and any future models that are developed.

9. Acknowledgements

The field measurements and data processing described in this report were supported by an interagency agreement between the U. S. Air Force and the Atmospheric Turbulence and Diffusion Division of NOAA 's Air Resources Laboratory.

References

- Aerospace Corporation, 1997a: Ground cloud dispersion measurements during the Titan IV Mission #K15 (5 December 1995) at Vandenberg Air Force Base—vol. 1 test overview and data summary. Aerospace Report TR-97(1410)-3, The Aerospace Corporation, El Segundo, CA, 146 pp.
- , 1997b: Ground cloud dispersion measurements during the Titan IV Mission #K24 (23 February 1997) at Cape Canaveral Air Station—vol. 1 test overview and data summary. Aerospace Report TR-97(1410)-7, The Aerospace Corporation, El Segundo, CA, 75 pp.
- Arritt, R. W., 1993: Effects of the large-scale flow on characteristic features of the sea breeze. *J. Appl. Meteor.*, **32**, 116–125.
- Atkins, N. T. and R. M. Wakimoto, 1997: Influence of the synoptic-scale flow on sea breezes observed during CaPE. *Mon. Wea. Rev.*, **125**, 2112–2130.
- Atkins, N. T., R. M. Wakimoto, and T. M. Weckwerth, 1995: Observations of the sea-breeze front during CaPE. part II: Dual-Doppler and aircraft analysis. *Mon. Wea. Rev.*, **123**, 944–969.
- Auble, D. L. and T. P. Meyers, 1992: An open path, fast response infrared absorption gas analyzer for H₂O and CO₂. *Bound.-Layer Meteor.*, **59**, 243–256.
- Bjorklund, J. R., 1990: User's manual for the REEDM Version 7 (Rocket Exhaust Effluent Diffusion Model) computer program. Technical Report TR-90-157-01, H. E. Cramer Company, Inc., prepared for Eastern Space and Missile Center, Patrick Air Force Base, FL, 279 pp.
- Brown, E. N., C. A. Friehe, and D. H. Lenschow, 1983: The use of pressure fluctuations on the nose of an aircraft for measuring air motion. *J. Climate Appl. Meteor.*, **22**, 171–180.
- Byers, H. R. and H. R. Rodebush, 1948: Causes of thunderstorms of the Florida Peninsula. *J. Meteor.*, **5**, 275–280.
- Crawford, T. L. and R. J. Dobosy, 1992: A sensitive fast-response probe to measure turbulence and heat flux from any airplane. *Bound.-Layer Meteor.*, **59**, 257–278.
- Crawford, T. L., R. T. McMillen, and R. J. Dobosy, 1990: Development of a “generic” mobile flux platform with demonstration on a small airplane. NOAA Technical Memorandum ERL ARL-184, NOAA Air Resources Laboratory, Silver Spring, Maryland, 60 pp.
- Eckman, R. M., C. J. Nappo, and K. S. Rao, 1996: Rocket Exhaust Effluent Diffusion Model (REEDM) verification and sensitivity study. NOAA Technical Memorandum ERL ARL-214, NOAA Air Resources Laboratory, Silver Spring, Maryland, 56 pp.

- Kamada, R. F., G. E. Start, R. P. Hosker, Jr., J. T. Knudtson, and H. L. Lundblad, 1997: MVP: Elevated SF₆ puff/plume releases from 1–1200 m at Cape Canaveral, FL. In *Proceedings of the Sixth Topical Meeting on Emergency Preparedness and Response, Vol. 1*, American Nuclear Society, 43–46.
- Kruczynski, L. R., D. G. Porter, and E. T. Weston, 1985: Global Positioning System differential navigation test at the Yuma Proving Ground. *Navig.*, **32**, 126–133.
- Leick, A., 1990: *GPS Satellite Surveying*. John Wiley & Sons, New York.
- Leise, J. A. and J. M. Masters, 1991: Wind measurement from aircraft, draft report, NOAA Aircraft Operations Center, Miami, FL.
- Lenschow, D. H., 1986: Aircraft measurements in the boundary layer. In *Probing the Atmospheric Boundary Layer*, D. H. Lenschow, ed., American Meteorological Society, Boston, MA, 39–55.
- Neumann, C. J., 1971: The thunderstorm forecasting system at the Kennedy Space Center. *J. Appl. Meteor.*, **10**, 921–936.
- Reed, J. W., 1979: Cape Canaveral sea breezes. *J. Appl. Meteor.*, **18**, 231–235.
- Rew, R., G. Davis, S. Emmerson, and H. Davis, 1997: NetCDF user’s guide for C. Technical report, Unidata Program Center, University Corporation for Atmospheric Research, Boulder, Colorado, 148 pp.
- Simpson, J. E., 1994: *Sea Breeze and Local Winds*. Cambridge University Press, Cambridge, United Kingdom.
- Start, G. E. and D. Hoover, 1995: Model validation program, Cape Canaveral, Florida, draft report, NOAA Air Resources Laboratory, Field Research Division, Idaho Falls, ID.
- Taylor, G. E., C. R. Parks, M. K. Atchison, G. W. Drapé, A. Dianic, D. Nuggent, W. Jubach, and H. Firstenberg, 1989: KABLE data analysis and EMERGE sea breeze algorithm evaluation. Report ARS-MPR-89-23, ENSCO, Inc., Melbourne, FL.
- Wallace, J. M. and P. V. Hobbs, 1977: *Atmospheric Science, An Introductory Survey*. Academic Press, New York.
- Zhong, S. and E. S. Takle, 1992: An observational study of sea- and land-breeze circulation in an area of complex coastal heating. *J. Appl. Meteor.*, **31**, 1426–1438.
- Zhong, S., J. M. Leone, Jr., and E. S. Takle, 1991: Interaction of the sea breeze with a river breeze in an area of complex coastal heating. *Bound.-Layer Meteor.*, **56**, 101–139.